Worst-Case Severe Environments for Surface Charging observed at LANL satellites as Dependent on Solar Wind and Geomagnetic Conditions

N. Yu. Ganushkina[1,2], B. Swiger[1], S. Dubyagin[2], J.-C. Matéo-Vélez[3], M. W. Liemohn[1], A. Sicard[3], D. Payan[4]

[1]University of Michigan, Ann Arbor, Michigan, USA.
[2]Finnish Meteorological Institute, Helsinki, Finland.
[3]ONERA - The French Aerospace Lab, Toulouse, France.
[4]Centre National dEtudes Spatiales, Toulouse, France.

Key Points:

- Presence, but not magnitude, of substorm activity as shown by AE (AL) index is the strongest characteristics for severe environments for surface charging
- Occurrence of even a moderate storm is not necessary for severe environments for surface charging to occur
- Solar wind velocity and its magnitude is a direct indicator for the highest risk of severe environments for surface charging

Corresponding author: Natalia Ganushkina, ganuna@umich.edu

Abstract

The 400 worst-case severe environments for surface charging detected at LANL satellites during the years of 1990-2005 as binned by the definitions of four criteria developed by Matéo-Vélez et al. (2018) and the solar wind and IMF parameters and geomagnetic activity indices are analyzed. The conducted analysis shows that only AE (AL) index determines the highest risk for severe environments for surface charging to happen. The presence of a substorm with the southward turning pattern in IMF B_z indicates that the environment can be severe for surface charging to occur but this environment will not depend on whether a substorm was moderate or intense. No clear dependence on IMF B_z is found for risk to a severe environment to occur. Appearances of severe environments for surface charging do not necessarily require high values of Kp and no storm is needed for such an event to be detected. Among solar wind parameters, solar wind velocity V_{sw} is directly related to the highest risk of severe environments, dependent on the V_{sw} value; and number density N_{sw} is of no importance. Two criteria for severe environment events based on the enhancements of low energy particle fluxes exhibit clearer dependencies on the solar wind and IMF parameters and geomagnetic activity indices with more distinct patterns in their time history.

Plain Language Summary

In spite of recent engineering and technological advancements, modern satellites are still subject to dangerous influence from radiation due to presence of high energy particles in the near-Earth space. These particles can cause accumulation of some charge on the satellites surfaces. They vary a lot depending on the activity on the Sun. The solar activity can be characterized by several parameters. Relating the detected surface charging events to the parameters can help to predict the occurrence of these events based on knowing the solar activity. The 400 worst-case severe environments for surface charging detected at Los Alamos National Laboratory satellites during the years of 1990-2005 were analyzed and related to solar activity. It was found that surface charging can occur during rather moderately disturbed conditions, and presence of a strong disturbance does not necessarily lead to satellite anomalies. Solar wind velocity and its magnitude can be a direct indicator for the highest risk of severe environments for surface charging.

1 Introduction

In spite of recent engineering and technological advancements since previous analyses of spacecraft anomalies (e.g., Vampola, 1994; Koons et al., 1999), modern satellites are still subject to environmental effects (e.g., Green et al., 2017). Spacecraft charging causes the most spacecraft anomalies related to the radiation environment (e.g., Lam et al., 2012; Loto'aniu et al., 2015), and it is surface charging in particular that has caused more serious ones (e.g., Koons et al., 2000; Choi et al., 2011; Matéo-Vélez et al., 2018).

Surface charging is due to low energy plasma and photoelectric currents (for details, see the reviews by e.g., Garrett (1981); Whipple (1981); Mikaelian (2001)). The spacecraft surface potential is a function of the net current to/from the spacecraft surface. The net current consists of currents from (1) photoelectrons from the surface induced by solar photons, (2) electrons and ions of surrounding plasma impinging on the surface, and (3) charged particles emitted from the satellite (e.g., from electron emission induced by primary electrons, from active ion emission). In a balance, a net current is equal to zero. A spacecraft submerged into plasma will assume a floating potential different from the plasma itself. The net current between the surfaces and the plasma will tend to become zero, therefore, the satellite's surface materials will be charged oppositely to the surrounding plasma. The shadowed areas are charged negative. The sunlit areas are charged positive unless some negative barrier of potential (also given by absolute spacecraft potential) imposed by other satellite's surfaces prevent photoelectron to reach the plasma. Even in this case, however, sunlit surfaces remain less negative than other surfaces. For the conducting surfaces, the potential of the surface is uniform for reaching the equilibrium for zero net current. For insulating materials, this equilibrium can be only on several points on the surface. Surface materials can discharge both into space and/or to structure ground. The resulting electrostatic discharge (ESD), with conducted currents and/or radiated waves, can couple into electronic circuits and subsystems, causing damage. Spacecraft charging is a function of the space environment characteristics, including sunlight/eclipse, solar activity, geomagnetic activity, electron and ion flux magnitude and spectrum.

The electron temperature is considered the most reliable space environment parameter to predict spacecraft charging based on observational (Rubin et al., 1980; Lai & Della-Rose, 2001; Lai & Tautz, 2006) and theoretical (Lai et al., 1983; Hastings & Garrett, 1996)

evidence. The spacecraft potential and electron temperature curves show an intercept at a finite temperature. When temperature is below this critical value, spacecraft charging does not occur, it starts only with temperature above it.

Olsen (1983) demonstrated the existence of a threshold energy of 10 keV (kiloelectronVolt) of particle fluxes for the SCATHA (Spacecraft Charging At High Altitudes) spacecraft to charge when a large portion of the ambient electron flux exceeds this energy. A later study by Thomsen et al. (2013) for LANL (Los Alamos National Laboratory) MPA (Magnetospheric Plasma Analyzer) data showed that surface charging will occur when a critical threshold of electron fluxes with energies of 8 keV has been satisfied. Sarno-Smith et al. (2016) analyzed the relationships between 30 eV - 50 keV electron fluxes and spacecraft potential using Van Allen Probes HOPE (Helium Oxygen Proton Electron) and EFW (Electric Field and Waves) data. They found the electron energy flux threshold for 3 keV electrons for intense charging more likely to occur, however, they stated that it is not always the case. In addition, the electron pressure, not the average electron temperature was shown to have stronger connection to spacecraft charging; but, again, this correlation was not always present. In the studies mentioned above, the spacecraft potential was obtained from observations of the "ion line" (e.g., Thomsen et al., 2013) which represents a sharp low-energy cutoff due to the acceleration of ambient ions through the spacecraft potential.

Correlation between spacecraft anomalies and substorm activity was observed in the 1970s on the ATS (Applications Technology Satellite)-5 and -6 and the first two Defense Satellite Communication System-Phase II (DSCS-II) geosynchronous communication satellites using magnetometer data from ground stations near the satellite magnetic footprint (Rosen et al., 1972; Fredricks & Scarf, 1973). DeForest (1972) directly demonstrated that the surface of the ATS-5 spacecraft was charged to large negative potentials (up to -9 kV (kiloVolt) under eclipse conditions), when the spacecraft was in the local morning sector, by $\sim$ 1-10 keV electrons injected from the plasma sheet during substorm-associated events. Farthing et al. (1982) analyzed the ground magnetograms from Anchorage station in Alaska and found that the substorm activity occurred very closely in time with the anomalies detected at GOES (Geostationary Operational Environmental Satellite) 4 and 5 in the postmidnight sector. Extended analysis of data from ATS-6, GEOS (Geodetic Earth Orbiting Satellite)-2 and SCATHA resulted in the design guidelines (Purvis et al., 1984) for mitigation of the differential charging hazard. Spence et al. (1993) in-

vestigated about 100 anomalies that occurred at several high-inclination, high-altitude satellites by comparing their distribution to the known surface charging distributions (i.e. observed an SCATHA spacecraft) and related them to 10-15 keV energetic particle injections from the Earth's magnetotail during substorms.

The satellite anomalies caused by substorm injection depend on local time indicating that they were caused by geomagnetic activity but not by operational or design problems. Numerous studies (e.g., Koons & Gorney, 1991; Spence et al., 1993; Lanzerotti et al., 1998; Fennell et al., 2001; Gubby & Evans, 2002; Iucci et al., 2006; O'Brien, 2009; Allen, 2010; Choi et al., 2011; Mazur et al., 2012) showed that surface discharges peak at around midnight to dawn in local time with very few occurring on the dayside. That is, the anomalies are the most frequent in the sector of substorm electron injections. For example, Fennell et al. (2001) have analyzed the occurrences of anomalies on HEO (Highly Elliptical Orbit) satellites (Spence et al., 1993) and found that the spatial distribution of the HEO anomalies mapped to the equatorial plane is close to the pattern of substorm-injected electrons. On the contrary, the effects of internal charging should be most prominent on the dayside or should show no local time dependence at all (Mazur & O'Brien, 2012).

At the same time, it is not possible to state that all substorms and, especially, intense ones, will definitely lead to satellite anomalies and that they will be due to surface charging. Small, isolated substorms can be related to the significant changes in the radiation environment which could lead to the surface charging related anomalies (e.g., Grafodatskiy et al., 1987; Matéo-Vélez et al., 2016). Matéo-Vélez et al. (2018) have examined the particle data from the LANL spacecraft and extracted times when the particle environment can be extreme and can result in surface charging conditions. It was shown (see Figure 8 in Matéo-Vélez et al. (2018)) that severe conditions can occur during geomagnetic storms or isolated substorms but the occurrence even of a moderate storm is not necessary. All the identified times (400 of them) with severe particle environments were attributed with the values of Dst (Disturbance storm time) and AE (Auroral Electrojet) indices. Storms were identified by corresponding Dst variations seen as the initial, main and recovery phases but not by the strength of them. Isolated moderate substorms were defined by the AE index from 300 nT to 800 nT, isolated intense substorms – by AE-index higher than 800 nT, and small substorms with AE$<$ 300 nT. Many of the identified events in Matéo-Vélez et al. (2018) were detected during small to moderate

substorm activity, and no direct dependence was found on substorm strength. Most events in the Matéo-Vélez et al. (2018) study were observed in the 21-06 MLT (Magnetic Local Time) sector with very few in the <20 MLT or >07 MLT sectors, which is consistent with previous studies (e.g., Mullen et al., 1986).

Among multiple characteristics of geomagnetic activity, the Kp (Planetarische Kennziffer) index has been considered as the main geomagnetic index in the studies relating satellite anomalies with geomagnetic activity in early studies. Rubin and Garrett (1979) discovered the relation of ATS-5 and ATS-6 potential with Kp. Farthing et al. (1982) presented the correlation of the anomalies at GOES 4 and 5 spacecraft with the Kp. The positive correlation between the SCATHA satellite surface potential monitors (SSPMs) data and the Kp index was demonstrated by Mullen et al. (1986) and Koons and Gorney (1991). Later, Spence et al. (1993) analyzed about 100 anomalies detected at several high-inclination, high-altitude satellites and found that the anomaly occurrence is strongly related to the Kp index value. Choi et al. (2011) selected 95 anomalies that occurred at geostationary satellites from 1997 to 2009 and showed the anomaly occurrence rate increased with increase of the Kp index. Thomsen et al. (2013) found "an enhanced surface charging probability" at LANL satellites during higher Kp values. At the same time, the anomalies included the effects from both surface and internal discharges, which have similar dependence on the Kp index (Koons & Gorney, 1991).

However, no agreement was reached on a linear dependence between the anomalies which might be due to surface charging and the Kp value. While O'Brien (2009) stated that anomalies due to surface charging are most probable at Kp of 46, Denton and Borovsky (2012) found > 500 V spacecraft potentials occurring at relatively low Kp values of 2 or 3. O'Brien (2009) used the data of surface charge monitors (Ozkul et al., 2001; Koons et al., 2006) on geosynchronous satellites. Denton and Borovsky (2012) derived spacecraft potentials from the LANL particle data.

Lohmeyer and Cahoy (2013) analyzed 26 solid-state power amplifier (SSPA) anomalies detected at eight Inmarsat geostationary communications satellites during 1996-2012 and found that 80% of anomalies occurred with Kp < 3. Mazur et al. (2012) have analyzed statistics on surface charging signatures from a charging plate analyzer (CPA) observed on the Intelsat satellites (Koons et al., 2006) at GEO during 1997-2001. Charging potentials from CPA were more straightforward indication of surface charging than

obtaining a more complex charging signature from ion spectrograms (as was done in Thomsen et al. (2013)). Mazur et al. (2012) noticed that surface charging occurred during both quiet and active time intervals as seen in Kp index. Moreover, they found the influence from the RussellMcPherron effect (Russell & McPherron, 1973) with semiannual variations in the charging signatures, such as, together with Kp, the surface charging was more likely to happen during the spring and fall equinoxes (similar to the Matéo-Vélez et al. (2018) study).

Bodeau (2015) questioned the usage of the Kp index as an indicator for severe environments to cause surface charging and to induce anomalies due to it. A series of solar array string failures occurred on three high-power communication satellites (Hoeber et al., 1998) were compared with the Kp index and no dependence was found. The conclusion was that "a high Kp does not insure significant charging levels, and conversely, significant charging can occur during modest to severe Kp index values." Bodeau (2015) examined ground magnetograms and X-ray emissions measured by the Polar spacecraft from the atmosphere in the auroral region near the magnetic footprint of the communication satellites and found that severe substorm activity was detected right before nearly every moment of circuit failure.

Ferguson et al. (2015), while admitting that Kp dependence for surface charging seems to be logical, since Kp is an indicator of a disturbed magnetosphere, did not find any correlation trend between the LANL negative spacecraft potential and the large Kp values from 7 to 9 (see their Figure 38). They presented the electron flux above a minimum energy E_{min} as a charging index for geosynchronous spacecraft in sunlight with E_{min} of 9-15 keV and the threshold for flux above E_{min} to be near $4 \times 10^8\ e^-/cm^2 s$. The proposed observational charging index was later found to be consistent with the theory in the Huang et al. (2017) study.

While the Kp index has been extensively used in attempts to find correlations with surface charging anomalies, other characteristics, such as, the AE (Auroral Electrojet) and Dst (Disturbance storm time) indices and solar wind and IMF (Interplanetary Magnetic Field) parameters, were not. Wrenn and Smith (1996) estimated the probability of surface ESD effects on the MARECS-A satellite launched in 1981 at GEO as dependent on Kp and AE indices. They found that the probability to observe the effects from surface ESD increases for Kp from 3 to 5 and AE from 200 to 800 nT but decreases for

higher magnitudes of Kp and AE. This behavior was attributed to the magnetic field at GEO being drastically distorted. Lohmeyer et al. (2012) attempted to relate the Inmarsat anomalies with the Dst index and the solar wind speed and found that at the times of the anomalies, the Dst index did not drop below -40 nT and the solar wind speed varied in the range between 300 and 500 km/s exceeding 600 km/s at only two times (see their Figure 14). The importance of the solar wind speed increase for spacecraft potential was reported in earlier studies (DeForest, 1972; Hastings & Garrett, 1996). Denton and Borovsky (2012) investigated spacecraft potentials at LANL during strong and weak High Speed Streams (HSS). They defined strong events when the solar wind speed is higher than 500 km/s during 5 days but weak events are characterized by the solar wind speed below 400 km/s during 3 days. Denton and Borovsky (2012) found a strong correlation between the average negative spacecraft potential and the solar wind speed. Moreover, the level of the corresponding surface charging was found to be significantly larger for the strong HSSs than for the weak HSSs.

In the present paper, we analyze a database of 400 events developed by Matéo-Vélez et al. (2018) (presented in Section 2) which contains the dates and times of the worst-case severe environments for surface charging as observed by LANL satellites during the years of 1990-2005. The main focus is to find possible relations between the activity parameters and worst-case severe environments for surface charging. Each input in the database was attributed with the corresponding values of geomagnetic activity indices and solar wind and IMF parameters. The dependencies of worst-case severe environments for surface charging and near-simultaneous geomagnetic activity are contained in Section 3. It shows peaks in the number of events with corresponding parameter magnitude and range, the highest risk to detect a worst-case severe environment event at the corresponding value of the parameter, and presence of a risk-parameter dependence. Section 4 demonstrates the results of a superimposed epoch analysis with the parameter changes in time before the event, relative timing of parameter maximum change and the event detection time moment, and parameter changes after the event. The obtained dependencies are discussed, and the conclusions are drawn in Section 5.

2 Severe Environment Events from LANL Data

We use the database of 400 total events developed by Matéo-Vélez et al. (2018) that contains the dates and times of the worst-case severe environments for surface charging

as observed by LANL satellites during the years of 1990-2005. Matéo-Vélez et al. (2018) have analyzed the particle fluxes from the MPA with energies from 100 eV to 40 keV (Bame et al., 1993), the Synchronous Orbit Particle Analyzer (SOPA) with energies between 50 keV and 1.3 MeV (Belian et al., 1992) and the Energetic Spectra for Particles (ESP) with energies from 1 to several MeV (Meier et al., 1996). Matéo-Vélez et al. (2018) have formulated four different criteria to define severe environments potentially leading to surface charging. 100 worst case events were identified in each criterion with 400 events in total. For a given criterion, each event is among the top 100, 15-minuted averaged worst-case severe environments for surface charging defined by that criterion. These four groups of events comprise the main dataset of our study. They also form the basis of on-ground tests of materials under multi-energetic electron beams (Matéo-Vélez et al., 2019).

Among the four criteria, one criterion is based on the measured spacecraft potential and three criteria are based on integral electron fluxes. The spacecraft potential criterion deals with the average spectra related to large negative potentials over long periods of time. It was called PG5k, since the longest events with a Potential Greater than 5 kV (in absolute) were considered. The criterion defines 100 longest events with Potential Grater than 5 kV (in absolute). It should be stressed that the top 100 events are selected on the basis of duration of the potential drop rather than the potential drop peak value. This means that the events with stronger charging but having shorter duration are dismissed by this criterion. On the other hand, the threshold values of -5 kV used for the event definition obviously represents extreme charging.

Eclipse or sunlit conditions play a very important role in PG5k criterion. Photoemission is generally the most important charging current, which is able to counterbalance a large fraction of the negative current imposed by electron fluxes during substorms, depending on the incidence angle of photons on the satellite's surfaces. In the present study, 87 out of the 100 PG5k worst-cases are in eclipse. Therefore, it can be considered that PG5k worst-case environments are representative of the most severe charging events occurring during eclipse. The dependence of these events on plasma and geomagnetic conditions is very interesting issue because they are less subject to the uncertainties linked to the sunlight incidence on satellite surfaces.

For criteria based on fluxes, the electron fluxes have been averaged over 15 minutes, since it is necessary for severe conditions to be present for a few minutes for dif-

ferential charging to occur at geosynchronous orbit. Matéo-Vélez et al. (2018) used 15 minutes as an approximate duration to bring significant differential charging (hundreds of volts) on dielectrics of about 25 to 100 μm thickness in a GEO-like environment.

One criterion concerns high fluxes at low energies together with a Low Flux at High Energy (LFHE). It is a combination of both high fluxes below 50 keV and low fluxes above 200 keV which is related to surface charging. Another criterion concerns the Highest Fluxes at All Energies (HFAE). It combines high fluxes both below 50 keV and above 200 keV, since they are related to charge deposited both at the surface and in the bulk of covering insulators. The last criterion is about the highest Fluxes of electrons at Energies above 10 keV (FE10k). The most severe electron spectrum was selected each month on each spacecraft to avoid duplication if the same events were detected by several spacecraft. The list of most severe satellite-month spectra was then classified within top 100 events, one for each criterion, resulting in 400 events in total. A potential below -300 V was reached for 80 FE10k worst-case events out of 100, 60 for HFAE and 40 for LFHE. It should be stressed here that the worst-case environments criteria were defined to address both absolute negative potentials and large differential potential at the same time. This is generally speaking a difficult task because LANL data can be used to compute absolute potential but not differential. Therefore, Matéo-Vélez et al. (2016) proposed different ways to define a worst-case depending on the relative importance of low and high energy electron fluxes. The best correlation with absolute charging was obtained with PG5k, of course, by definition, and with FE10k. However, LFHE and HFAE should not be dismissed because, first, a large fraction of them was associated with potential below -100 V, and, second, they can theoretically generate high levels of differential charging levels due to specific interaction of electrons with insulators. This is why all these 4 criteria are relevant for the present study with the goal to assess risks of surface charging leading possibly to electrostatic discharges and, in the end, to spacecraft anomalies.

Each event in all 400 events was attributed with the corresponding values of Kp, AE, AL (Auroral Lower), and SYM-H (symmetric disturbance magnetic field in H-component) indices and solar wind and IMF parameters, namely, IMF B_Z, solar wind speed, proton number density, and derived electric field E_y and $<VB_s>$. For solar wind and IMF data, OMNIWeb (http://omniweb.gsfc.nasa.gov/) was used, so, E_y was obtained directly from there and $<VB_s>$ was computed using solar wind speed and B_s, defined as $B_s =\mid B_z \mid$, if B_z is negative and $B_s = 0$ otherwise. Geomagnetic indices were obtained from the

World Data Center for Geomagnetism, Kyoto (http://wdc.kugi.kyoto-u.ac.jp/wdc/Sec3.html). The dependencies on solar wind and IMF parameters and geomagnetic indices of the events in each criterion were then studied.

3 Worst-Case Severe Environments for Surface Charging and Current Geomagnetic Activity

3.1 Dependence on Geomagnetic Indices

3.1.1 Kp Index

We start with dependencies on geomagnetic indices. The four top panels in Figure 1a present the histograms of top 100 events with worst-case severe environments for surface charging as dependent on the Kp index observed during these events. These severe environment events in 15-minute intervals were identified by Matéo-Vélez et al. (2018) following the criteria PG5k (top panel, purple), LFHE (second panel, green), HFAE (third panel, red), and FE10k (forth panel, blue). The Kp index occurrence rate (orange line) for the entire period of 1990-2005 (irrespective of the environment condition) is shown in the bottom panel. The Kp binning was done so that the [0,1) bin includes Kp values of 0, 0+, and 1-, the [1, 2) bin includes Kp=1, 1+, and 2-, and so on, and the [8, 9] bin includes Kp=8, 8+, 9-, and 9.

Several features can be noticed in the plotted histograms:

(1) The histograms showing the number of severe environment events in all four criteria do not coincide with the 16 years occurrence rate of the Kp index (orange line in the bottom panel). The highest occurrence rate for the observed Kp is from 1 to 3. If they would have coincided, for each Kp value, the probability of the presence of a severe environment would be the same, independent of Kp. Since this is not the case, the Kp value can be considered as an indicator for an event to happen.

(2) The PG5k histogram, which corresponds to the spacecraft potential criterion, has its peak at Kp = 3-4 (39 events), whereas all the histograms for criteria based on electron fluxes show maximum values at Kp = 4-5 (25-30 events), except for HFAE criterion which has a wider peak at Kp = 3-5.

(3) There are more PG5k events at smaller Kp (6 events at Kp = 1-2 and 20 events at Kp = 2-3) as compared to flux based events with negligible number at Kp = 1-2 and 5-11 events at Kp = 2-3). (4) More events with flux based criteria occurred at higher

Kp (> 5) than those of spacecraft potential based criterion: there were ≤ 6 PG5k events in each Kp bin for Kp $>$ 5, whereas 18 LFHE and 20 FE10k events were detected at Kp = 5-7 and 19 HFAE events at Kp = 5-6. For large Kp > 7, only the FE10k criterion showed 16 (Kp = 7-8) and 8 (Kp = 8-9) events. Obviously, the Kp-dependent histograms for severe environment events do not reveal fully the risk to encounter the severe environment for given Kp: statistical decrease of the occurrence rate of higher Kp values (see bottom panel in Figure 1a) should be taken into account. In other words, the decrease in histograms for high Kp values during severe environment events may just reflect the lower probability of high Kp occurrence but not a lower risk of severe environment.

To address this issue, we developed a specific normalization procedure. The idea is to normalize the number of severe environment events for each Kp bin by the total number of LANL observations corresponding to this Kp bin. The only data analyzed in the present paper are the times and locations of 400 worst-case events, not the full, original LANL dataset (it was not freely available). What was available is the total numbers of 15 minute averages of the LANL observations in 20 to 08 MLT sector for different years used in Matéo-Vélez et al. (2018) given in Table 1. These numbers include all observations from all operating LANL spacecraft. The choice of 20 to 08 MLT sector is due to the finding that all of the worst-case severe environments were detected at local times from 20 to 08 MLT (see Figure 6b of Matéo-Vélez et al. (2018)). Thus, we calculate the chance to encounter the severe environment in the top 100 only for this MLT sector. The total number of LANL observations in a given Kp bin can be estimated by multiplying these numbers for the normalized Kp occurrence for given bin and year. In more details, the normalization algorithm can be explained as follows.

For a particular year, the number of events with detected top 100 worst-case severe environments for one particular Kp bin for all operating LANL spacecraft is $N_{eventsLANL}$. Let the total number of LANL 15 minute observations in 20-08 MLT sector be N_{LANL} (Table 1). To estimate the number of available LANL 15 minute observations for the particular Kp bin, the total number N_{LANL} must be multiplied by the occurrence rate $N_{Kp}norm$ (Figure 1a, bottom panel) of the Kp index for this bin for this year. $N_{Kp}norm$ is computed as $N_{Kp}/N_{Kp}all$, where N_{Kp} is the number of Kp records in a given Kp bin (at a given Kp value) for this year (irrespective of what LANL observes, just using the Kp

Year	1990	1991	1992	1993	1994	1995	1996	1997
# observations	13786	26044	34745	32117	26044	33284	42311	43627
Year	1998	1999	2000	2001	2002	2003	2004	2005
# observations	44925	53001	43439	39115	65062	69113	64823	53185

Table 1. Total numbers of 15 minute averages of the LANL observations in 20 to 08 MLT sector for different years from all LANL spacecraft used in Matéo-Vélez et al. (2018)

index distribution), and $N_{Kp}all$ is the total number of Kp records (number of 3 hour intervals in a year).

Now, for a given year, the normalized occurrence rate for an event in the list of top 100 severe environment events in a given Kp bin can be estimated as the number of severe events for a given Kp bin divided by the estimate for the number of all LANL observations for a given Kp bin:

$$Normalized\ occurrence\ rate = \frac{N_{eventsLANL}}{N_{Kp}norm \cdot N_{LANL}} \cdot 100\%. \quad (1)$$

To get the average risk (normalized occurrence rate), we sum over all years:

$$< Normalized\ occurrence\ rate >= \frac{\sum_{i=1990}^{2005} N_{eventsLANL_i}}{\sum_{i=1990}^{2005} N_{Kp}norm_i \cdot N_{LANL_i}} \cdot 100\%. \quad (2)$$

It should noted that this method of normalization does not perfectly suits to PG5k criterion events because almost all these events occurred in eclipse. This means that being in eclipse is a necessary condition to have such an event. Therefore, PG5k events should be normalized by the total time the spacecraft spends in eclipse for a given Kp bin. Since the eclipse conditions for GEO occur at around the equinoxes and the geomagnetic activity has semiannual variation (Russel-McPherron effect) (Russell & McPherron, 1973), it is impossible to do such normalization without the orbital information. For this reason, we estimate the risk to have PG5k event using the same method as for other criteria and keeping in mind this specific feature of PG5k events (duration of charging but not peak value). It should be emphasized that we define the risk as a chance to have one of 100 top events (but not to exceed certain threshold). For this reason, the PG5k risk values can be compared to the ones of other criteria.

The normalized severe environment occurrence rate is shown by black dots in the four top panels of Figure 1a. It is important to note that the normalized occurrence rate described above is different from that of shown in the bottom panel of Figure 1a. The black dots can be considered as an indicator of a risk to detect a top 100 worst-case severe environment event in a 15 min window for a given Kp bin.

The uncertainties for each normalized severe environment occurrence rate (black dot) are shown with vertical bars in Figure 1a-c. The uncertainties were calculated using the counting error as $\delta_Q = \sqrt{N_Q}$, where N_Q is the number of observations in the sample Q. When computing the uncertainties for the normalized occurrence rate given by Equation 2, we assume that the uncertainties from quantities in the denominator are negligible compared to those from $N_{eventsLANL}$. So, uncertainty δ of the risk for severe environment occurrence is:

$$\delta = \frac{\sqrt{\sum_{i=1990}^{2005} N_{eventsLANL_i}}}{\sum_{i=1990}^{2005} N_{Kp}norm_i \cdot N_{LANL_i}} \cdot 100\%. \tag{3}$$

As it can be noticed in Figure 1a-c, the uncertainties for Kp bins with less than 2 events (for Kp from 1 to 2 for LFHE and HFAE criteria, for Kp from 7 to 8 for PG5k and HFAE criteria and for Kp from 8 to 9 for HFAE criterion) have their lower limit as zero. Variations in both upper and lower limits in the uncertainty bars are important for determining a trend in the dependence of risks on the value of Kp. The risks which have their lower limit in the uncertainty bar equal to zero are considered much less significant and excluded when analyzing the dependencies.

The risk is different for each criterion (note that risk values for PG5k are not 100% directly comparable to other criteria). For PG5k, the highest risk (for all Kp bins with more than 1 events) to detect the severe environment is no more than 0.04% ± 0.008%, for LFHE, it is 0.2% ± 0.05%, for HFAE - 0.08% ± 0.02%, and for FE10k - 0.5% ± 0.2%. These numbers can look very small and give the impression that there is not whatsoever dependence of severe environment occurrence on any of Kp index value. It should be stressed particularly that while analyzing these numbers, it is important to keep in mind the definition of those selected 100 events in each criteria: only the top 100 15 minute-averaged worst-case severe environments. It is expected that the chance of getting the particular event out of only 100 selected at a certain time and spacecraft location for a partic-

ular Kp bin during 16 years cannot be high. The calculated uncertainties are much larger for higher Kp values when the number of events is very small. Overall, the smaller the number of events, the larger the uncertainty.

The analysis of risks shows the following:

(1) We see the order of magnitude difference in risks with the largest for FE10k criterion and smallest for PG5k criterion (keeping in mind eclipse events in PG5k criterion, see above).

(2) The only criterion which indicates an increase of observing severe environment with Kp increase is FE10k, highest fluxes of electrons at energies above 10 keV. All other criteria show the initial increase with Kp up to Kp = 4-5 and somewhat saturation at higher Kp. The trends in the uncertainties are in agreement with those of the risks. There are not so many events with Kp > 6-7 during all 16 years as the bottom panel shows. At the same time, the number of FE10k events for Kp > 6 is not small, therefore, worst-case severe environments can occur often when Kp is high, which is not true for other criteria.

The conducted analysis demonstrates that the magnetosphere needs to be in an active state (Kp > 2) for an event to happen but it is not necessarily true that a higher Kp value means that more events will be detected.

3.1.2 AE Index

Figure 1b demonstrates the relationships between the events with top 100 15 minute-averaged worst-case severe environments for surface charging and the AE index in a similar form as in Figure 1a for the Kp index. The values used to plot each histogram (first four panels) are the median AE index observed during ± 5 min from the start of the worst-case severe environment event. The bottom histogram (orange line) presents the AE occurrence rate computed for the entire period of 1990-2005 irrespective of the environment conditions. The values for black dots and uncertainties for them were computed similarly to those of the Kp index.

The uncertainties for the AE bins with no LANL events between the AE bins where events are present (for example, in Figure 1b, for AE from 1200 nT to 1300 nT and from 1400 nT to 1500 nT for PG5k criterion) are computed assuming that the LANL events

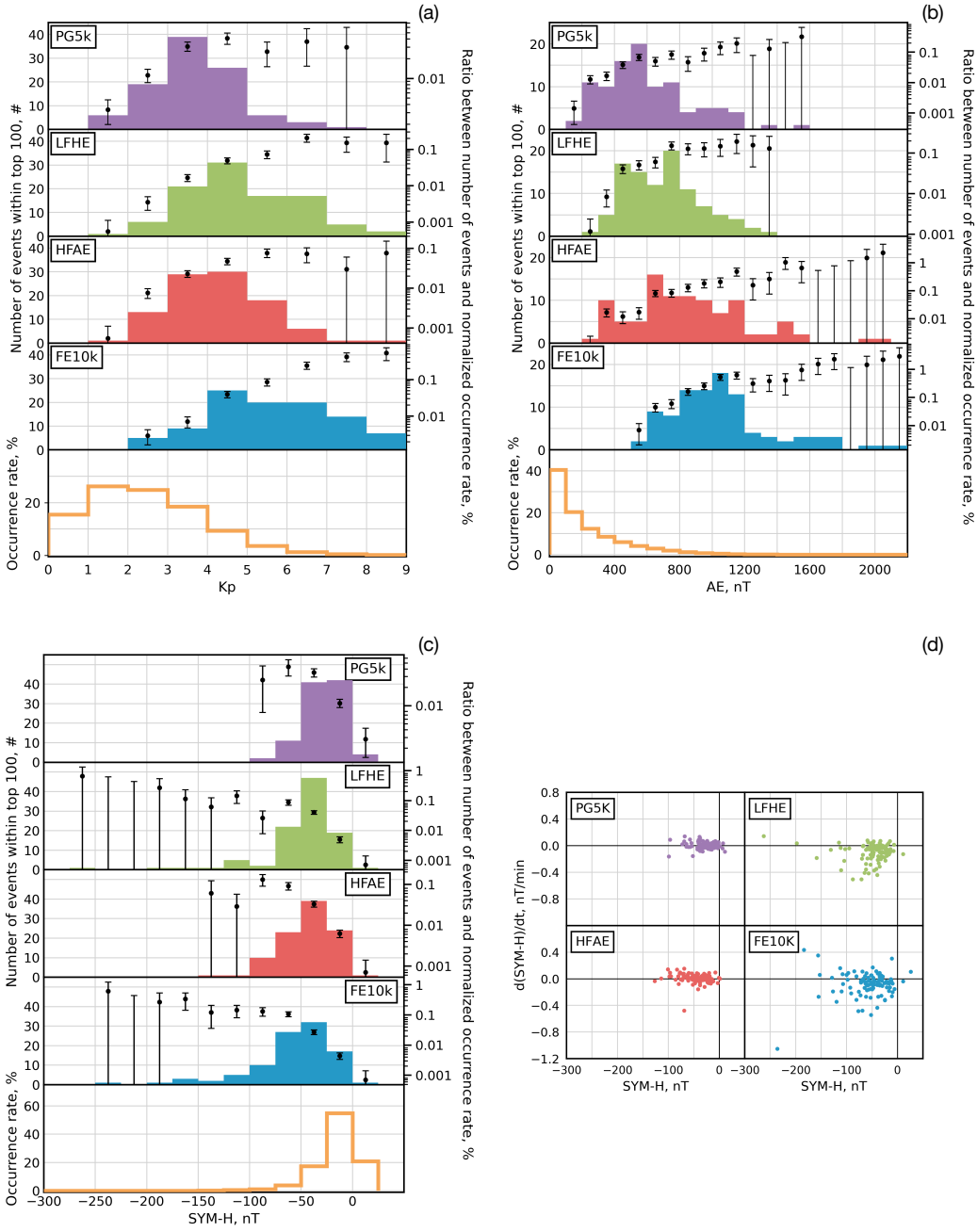

Figure 1. Number of events with top 100 15 minute-averaged worst-case severe environments for surface charging to occur for the criteria PG5k (top panel, purple), LFHE (second panel, green), HFAE (third panel, red), and FE10k (forth panel, blue) as dependent on the (a) Kp index, (b) AE index, and (c) SYM-H index. The occurrence rate (orange line) of the observed index for 1990-2005 is shown in the bottom panels. Black dots demonstrate the normalized severe environment occurrence rate with uncertainties shown as bars. (d) presents the d(SYM-H)/dt(SYM-H) versus SYM-H for all events for four criteria: Negative d(SYM-H)/dt values indicate the main phase of a storm (see the paper text for details).

count is zero with a counting error of one for that bin, and the risk uncertainty is calculated using a counting error of one, instead of zero. For these bins, we show the risk at zero with its estimated upper limit uncertainty bar, lower limit being zero. The computed uncertainties for such bins are not significant for analyzing the trends in the parameter dependencies.

Analyzing the plotted histograms, it can be noticed that:

(1) Similarly to the Kp index, the histograms showing the number of severe environment events in all four criteria do not coincide with the 16 years occurrence rate of the AE index (orange line in the bottom panel). The maximum occurrence rate of 40% occurs at AE = 0-100 nT with 20% at AE = 100-200 nT, which corresponds to an absence of substorm activity or rather small substorms, hence, the AE index can be considered as an indicator for an event to happen.

(2) The PG5k spacecraft potential criterion histogram peaks with 20 events at AE of 500-600 nT where about 10 events occurred in each bin with AE from 200 to 800 nT. For higher AE values of 800-1200 nT, the number of events is low, not more than 5 in each AE bin and almost no events for AE> 1200 nT. A rather different pattern can be seen on the flux-related FE10k criterion histogram, which has a peak of 18 events at AE of 1000-1100 nT with about 10 or more events in each AE bin for AE of 600 to 1200 nT. In contrast to the spacecraft potential criterion, there are events for AE>1200 nT (though, less than 5 in each AE bin but 20 in total). LFHE (20 events) and HFAE (15 events) criteria peaks are in the middle, being at 700-800 nT and 600-700 nT of AE, respectively. LFHE events of meaningful numbers occur when AE is between 300 and 1200 nT and for HFAE events this AE interval is 300-1600 nT - almost the same. Thus, similarly to Figure 1a, the FE10k environment is more likely to occur during increased magnetospheric activity compared to the other criteria.

(3) The normalized occurrence rate for severe environment events shown as black dots show that the highest risk to detect the severe environment is about one order of magnitude higher for three criteria, PG5k, HFAE and FE10k, when the AE index is elevated as compared to the Kp index. The highest percentage of 2.3% $\pm$ 1.3% is again for flux-related FE10k criterion. At the same time, for HFAE criterion, it is 1.0% $\pm$ 0.5% and for PG5k - 0.2% $\pm$ 0.1%. These are maximum values, but even if we look at the AE intervals with a meaningful number of events, the average percentages are still higher

than for the Kp index. Again, regardless of the small percentages, the maximum chance of getting the particular event out of only 100 selected at a certain time and spacecraft location for a particular AE bin during 16 years is one order of magnitude higher than for the Kp index.

(4) We cannot state that there is a linear increase of the highest risk to detect the severe environment with the increase of the AE index (taking all the risks with non-zero lower limit for corresponding uncertainty). Black dots for all criteria show a decrease with the decrease of the observed events for higher AE values, but largest substorm activity (as indicated by the large AE index values) results in the highest probability for a severe environment to develop. Substorm activity (represented by AE) is a more important factor than a general disturbed state of the magnetosphere (represented by Kp) for severe environments for surface charging to occur.

3.1.3 SYM-H Index

Figure 1c demonstrates the dependencies of the events with top 100 15 minute-averaged worst-case severe environments for surface charging on the SYM-H index in a similar form as in Figure 1a for the Kp index and in Figure 1b for the AE index. The values for SYM-H at the first four panels are the median values of SYM-H from ± 10 min from the start of the worst-case severe environment event. The bottom histogram (orange line) shows the SYM-H occurrence rate similarly to Figure 1a for Kp. The black dots and uncertainties for them were computed in the same way as in Figure 1a for Kp index. The main features are the followings.

(1) The histograms showing the number of severe environment events in three criteria based on electron fluxes do not coincide with the 16 years occurrence rate of the SYM-H index (orange line in the bottom panel). The maximum occurrence rate of 55% occurs at SYM-H between 0 and -25 nT which is not during storm times and only 20% at positive SYM-H = 0-25 nT and at SYM-H from -25 to -50 nT which can indicate small storm activity. LFHE (45 events), HFAE (40 events), and FE10k (32 events) histograms have their peaks at SYM-H from -25 to -50 nT, but there are 28 events in FE10k criterion at SYM-H from -50 to -75 nT. In contrast to other criteria, all events in spacecraft potential criterion PG5k were detected for SYM-H > -100 nT (40 events were seen in each SYM-H interval of 0 to -25 nT and -25 to -50 nT).

(2) As for Kp and AE indices, more events in FE10k criterion were detected for higher magnitudes of SYM-H as compared to other criteria, which indicates that these events occur during larger storms as compared to other criteria: about 45 out of the 100 FE10k events occur at SYM-H < -50 nT, 25 events for LFHE and about 35 for HFAE.

(3) The severe environment normalized occurrence rate in each bin (black dots) show increase for all the criteria up to SYM-H in the -50 to -75 nT range (-50 - -100 nT for HFAE) and then a drop for PG5k and LFHE criteria and with consequent increase for LFHE events. Again, we do not analyze the SYMH bins where only 1 event was detected which show an increase in risks for large negative SYM-H with zero lower limit for uncertainties. For the FE10k criterion, the dots reach a saturation for SYM-H from -50 to -150 nT and then increase. Since there are very few events at large negative SYM-H, we cannot conclude that more events will occur at strong storm times.

(4) The severe environment risk percentages are small: only 0.04% ± 0.01% for PG5k, 0.14% ± 0.06% for LFHE, 0.13% ± 0.04% for HFAE and 0.3% ± 0.2% for FE10k. These percentages are very similar and highest for LFHE and FE10k criteria as those of the Kp index dependencies. Out of three indices, the AE index is the best indicator of a severe environment for surface charging to occur.

Figure 1d presents the time derivative of the SYM-H index versus the SYM-H index during the top 100 severe environment events (each point corresponds to one event). Four panels correspond to events selected using different criteria. The values for SYM-H are the median values of SYM-H from ± 10 min from the start of the worst-case severe environment event. To calculate the SYM-H index derivative, we transformed the SYM-H time-series to the frequency space using the fast Fourier transform (FFT). The FFT was computed for a ∼34 h interval centered on the event time. Harmonics with a period <6 hours (frequencies greater than $50.0 \cdot 10^{-6}$ Hz) were zeroed, and a derivative was computed after inverse transformation. It is, therefore, a derivative of a smooth signal, where all short-scale variations (substorm-related) were filtered out. Negative large d(SYM-H)/dt values when the SYM-H index is strongly negative indicate that main phase of a storm was in progress during worst-case severe environment events. Positive d(SYM-H)/dt values at negative SYM-H correspond to the storm recovery phase.

As can be seen, the spacecraft potential based PG5k events are all concentrated within SYM-H > -100 nT with most points at 0 to -50 nT and corresponding d(SYM-

H)/dt values are ±0.15 nT/min which corresponds to rather small increases and decreases in SYM-H during the events but not to any significant storms. Strong storm activity does not result in severe environments for surface charging with PG5k criterion. Similar features are noticeable for HFAE criterion: although covering larger SYM-H interval from 0 to -125 nT, d(SYM-H)/dt was ± 0.2 nT/min and only one event with -0.45 nT/min at about -75 nT of SYM-H which can correspond to a main storm phase. There are more events with positive d(SYM-H)/dt which can be an indicator that HFAE events occur during small storm recovery. As can be seen in Figure 1c, PG5k and HFAE criteria have the lowest risk for detecting severe environments for any SYM-H index range.

For LFHE criterion, the majority of events is still situated at SYM-H from 0 to -75 nT but there are 9 events at SYM-H of -75 to -150 nT, most of the events have negative d(SYM-H)/dt with several reaching of about -0.4 to -0.5 nT/min which points to their occurrence during a storm main phase. It needs to be stressed here that the largest negative d(SYM-H)/dt values are still at SYM-H of -100 nT or more. FE10k criterion events are more distributed over SYM-H and d(SYM-H)/dt with many points concentrated at 0 to -75 nT of SYM-H but about the same number of them are with negative d(SYM-H)/dt values of -0.4 - -0.6 nT/min or more for SYM-H from 0 to -150 nT. One outlier is at -245 nT of SYM-H and with about -1 nT/min which corresponds to a strong storm. At the same time, about one third of all events are with positive d(SYM-H)/dt values but only 10 of them are during SYM-H <100 nT which indicates that FE10k events mainly occur during small and moderate storm recovery. Thus, most of the LFHE events can occur during the main phase of small to moderate (up to -150 nT) storms. This is true for the FE10k events, although FE10k events can also be detected during small to moderate storm recovery phase.

3.2 Dependence on IMF and Solar Wind Parameters

3.2.1 IMF B_Z

Figure 2a presents, in a similar way as Figures 1a-c, the histograms of the top 100 events with worst-case severe environments for surface charging as dependent on the IMF B_Z observed during these events. The values of IMF B_Z at the first four panels are the averaged values of IMF B_Z during one hour before the worst-case severe environment event. The bottom panel shows the histogram of the occurrence rate (orange line) of the

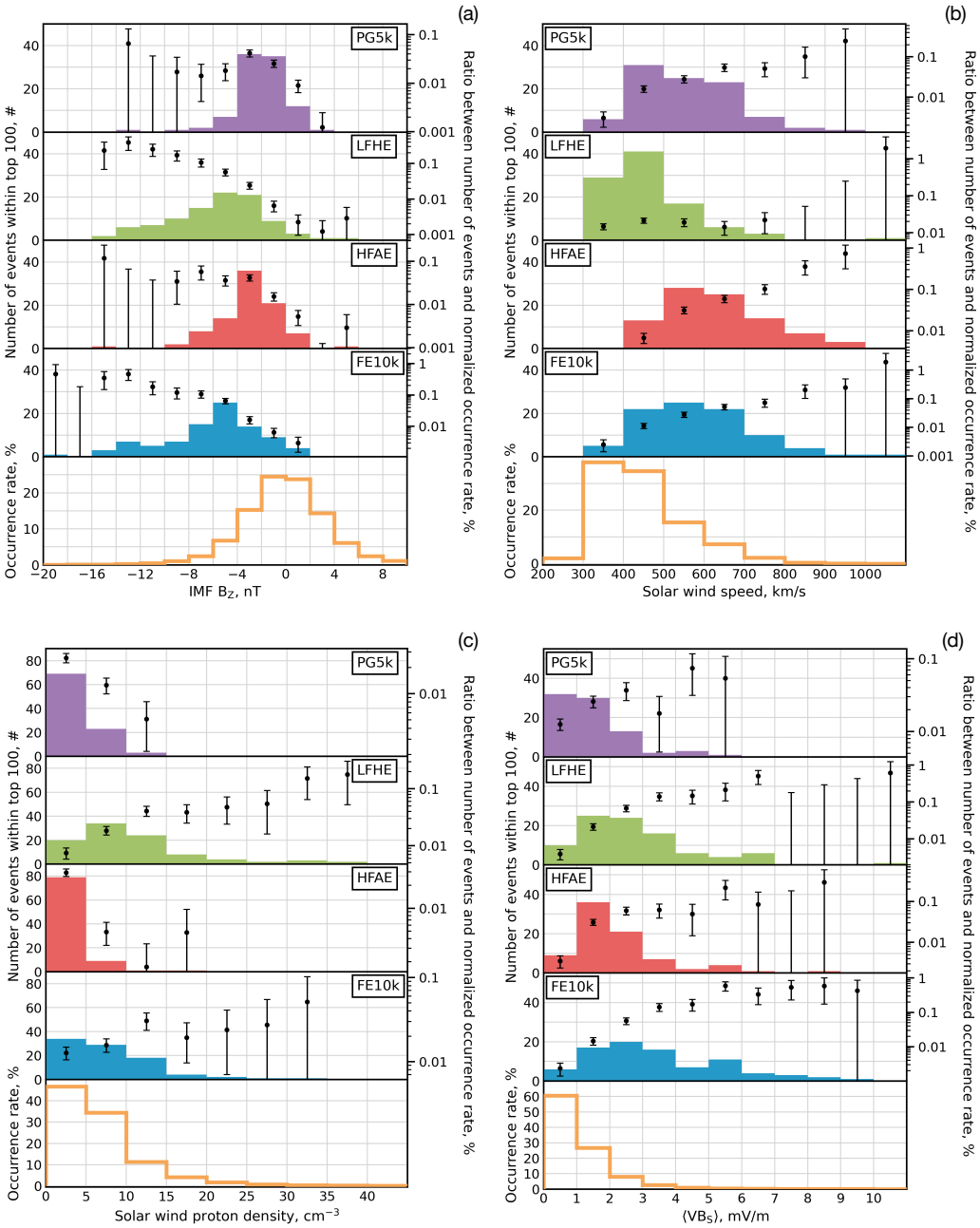

Figure 2. Similar to Figure 1, the number of events with top 100 15 minute-averaged worst-case severe environments for surface charging to occur for four criteria as dependent on the (a) IMF B_Z, (b) solar wind speed, (c) number density, and (d) $< \quad VB_s \quad >$ with the occurrence rate (bottom panel, orange) of the observed IMF and solar wind parameters for 1990-2005.

observed IMF B_Z for the entire period of 1990-2005 computed as the percentage ratio between the number of times when IMF B_Z fell into each bin (one bin is 2 nT) normalized by the total number of IMF B_Z observations during 1990-2005. The values for black dots and uncertainties for them were computed similarly as described for the Kp index (see Figure 1a description). IMF B_Z dependencies of the events of severe environments for surface charging show that:

(1) The occurrence rate (orange line) of the observed IMF B_Z has a symmetric shape in respect to IMF B_Z = 0 nT, with a maximum number at IMF $B_Z = \pm$ 2 nT. None of the histograms of each criterion has a similar peak location. This argues for the probability of detecting severe environments being dependent on IMF B_Z, so IMF B_Z can be considered as an factor influencing the occurrence of events. The histogram of the spacecraft potential based criterion PG5k shows a distinct, wider peak at IMF B_Z from 0 to -4 nT with 67 events for this IMF B_Z interval and <10 events for IMF $B_Z <$ -4 nT. The HFAE histogram also exhibits a pronounced peak with 36 events at -4 nT < IMF B_Z < -2 nT. Histograms for LFHE and FE10k show more distributed shapes, with a wider peak of 40 events at IMF B_Z from -2 nT to -6 nT and with 25 events at IMF B_Z from -4 nT to -6 nT, respectively.

(2) In addition to the peaks, the majority of the events for all criteria have occurred when the preceding hourly averaged IMF B_Z was negative. At the same time, there are about 25 events (out of 400) which occurred when the average IMF B_Z was positive. These events are present for each criteria with the largest number for PG5k, then HFAE, FE10k, and with the smallest number for LFHE. Since we used averaged values of IMF B_Z during one hour before each event to plot the histograms, IMF B_Z should have been predominantly positive during that hour before the event but not necessarily all positive.

(3) More events with LFHE and FE10k criteria have occurred at IMF $B_Z <$ -6 nT than for PG5k and HFAE criteria and they occur at -16 nT < IMF $B_Z <$ -8 nT when the number of PG5k and HFAE events were negligible.

(4) The risk to have severe environments represented by black dots with uncertainties increases with IMF B_Z becoming more negative for the LFHE and FE10k criteria but then it goes down in one IMF B_Z bin of -14 to -16 nT. For PG5k and HFAE criteria, there is no similar dependence: risk for PG5k criterion drops but for HFAE criterion it reaches some saturation at IMF $B_Z <$ -4 nT. The ratio percentages are small, though,

ranging from 0.04% ± 0.007% to 0.46% ± 0.18% and this is similar to those for Kp and SYM-H indices.

3.2.2 Solar Wind Speed

Similarly to Figure 2a, Figure 2b presents the dependencies of worst-case severe environments on the solar wind speed V_{SW}. The noticeable features are:

(1) The occurrence rate (orange line) of the observed V_{SW} has its maximum at V_{SW} = 300 - 500 km/s with higher rate at V_{SW} = 300 - 400 km/s. None of the histograms of each criterion has the exact same peak location, except the histogram for LFHE criterion peaks with 40 events at V_{SW} = 400 - 500 km/s and with 29 events at V_{SW} = 300 - 400 km/s. Other two criteria based on fluxes, HFAE and FE10k, do not exhibit any defined peaks in a specific V_{SW} interval with about 20 of events in each 100 km/s bin distributed over V_{SW} = 400-700 km/s for FE10k and 27-28 events each at V_{SW} = 500-700 km/s and 12 events each at V_{SW} = 400-500 and 700-800 km/s. The histogram of the spacecraft potential based criterion PG5k also shows a wider peak covering V_{SW} = 400-700 km/s with 30 to 23 events. V_{SW} can be considered as an factor influencing the occurrence of events.

(2) For higher V_{SW} = 700-900 km/s, there are more events corresponding to HFAE and FE10k criteria than with PG5k and LFHE.

(3) The risk to have severe environments represented by black dots with uncertainties increases with V_{SW} increase for PG5k, HFAE and FE10k criteria, reaching 0.1% ± 0.07%, 0.7% ± 0.4% and 0.2% ± 0.1%, respectively. These percentages are about order of magnitude higher than those for IMF B_Z. The only criterion which exhibits an order of magnitude lower risk, as compared to IMF B_Z is the LFHE one with a maximum value of 0.02% ± 0.003%. The risk for this criterion does not increase gradually with V_{SW} but dips into lower magnitude at V_{SW} = 600-700 km/s increasing again in the next V_{SW} interval.

In addition to the AE index, V_{SW} can be considered an indicator of a severe environment for surface charging to occur.

3.2.3 Solar Wind Proton Density

Figure 2c shows the histograms demonstrating the dependencies of worst-case severe environments on the solar wind number density N_{SW}. It can be seen that:

(1) Peaks of severe environment events for PG5k and HFAE criteria coincide with the maximum occurrence rate (orange line) of the observed N_{SW} at N_{SW} = 0-5 cm^{-3}. The occurrence rate decreases for larger values of the observed N_{SW}, so does the number of PG5k and HFAE events, with almost no events detected at $N_{SW} > 10$ cm^{-3}. The probability for a PG5k and HFAE event to happen does not depend on N_{SW}. The risk to have severe environments shown by black dots is about 0.03% ± 0.003% and decreases with the N_{SW} increase.

(2) Events with LFHE criterion show more distributed peak with 35 of them at N_{SW} = 5-10 cm^{-3} and with 20 each for N_{SW} = 0-5 and 10-15 cm^{-3}. 5-8 events were detected at larger N_{SW}, even at N_{SW} = 30-40 cm^{-3}. The risk to have severe environment for this criterion shown by black dots exhibits some gradual increase to only 0.05% at N_{SW} = 25-30 cm^{-3} with rise to 0.18% ± 0.13% at N_{SW} = 35-40 cm^{-3}. The percentage is about 2 times smaller than that for IMF B_Z but an order of magnitude larger than that for V_{SW} for the same criterion.

(3) About 35 events for the FE10k criterion were detected at N_{SW} = 0-5 cm^{-3} but in the following N_{SW} intervals, the number of events did not drop sharply as for the PG5k and HFAE criteria (with 19 events at N_{SW} = 10-15 cm^{-3} and non-zero number of events up to N_{SW} = 30-35 cm^{-3}). The risk to have severe environment for this criterion increases with N_{SW} increase with maximum percentage of 0.03% ± 0.007% which is about one of order magnitude smaller than that for IMF B_Z and V_{SW} for the same criterion.

Based on the analysis above, N_{SW} is not a good indicator of a severe environment for surface charging to occur.

3.2.4 $< VB_s >$

Figure 2d presents the dependencies of worst-case severe environments on $< VB_s >$, where V is the solar wind speed and B_s is equal to zero, when IMF $B_Z > 0$ and B_s = IMF B_Z, when IMF $B_Z \leq 0$. The $< VB_s >$ values in mV/m in the first four panels are one hour averages before the start of each event. The $< VB_s >$ values in the

bottom panel are calculated using a running one hour averages over the years of 1990-2005. Note that the first bin of $< VB_s >$ (0-1 mV/m) includes all zero values of B_s and all positive values of B_Z. Examining Figure 2d, it can be noticed that:

(1) The three criteria based on fluxes, LFHE, HFAE, and FE10k have their peaks at $< VB_s > > 1$ mV/m. That means that the preceding hourly averaged IMF B_Z was southward. LFHE criterion peaked with about 25 events in 1-3 mV/m bins, the HFAE criterion has a maximum of 35 events at $< VB_s >$ of 1-2 mV/m, and FE10k shows a more distributed peak with 18-20 events in each bin from 1 to 4 mV/m. For all three criteria, there are 10 or less events in the 0-1 mV/m bin. In contrast, PG5k criterion has about 30 events that occur in each of 0-1 and 1-2 mV/m bins. The occurrence rate (orange line) is highest at 0-1 mV/m.

(2) A severe environment defined by the PG5k criterion has the lowest risk (black dots) to occur, 0.07% $\pm$ 0.04%, among all four criteria. A large number of events in the 0-1 mV/m bin coinciding with highest occurrence rate over 1990-2005 years and no obvious dependence of the risk on the magnitude of $< VB_s >$ can be also seen.

(3) Events with LFHE criterion were detected over a wide range of $< VB_s >$ values, up to 7 mV/m, with one outlier event in the 10-11 mV/m bin. The risk for such an environment to occur is 0.5% $\pm$ 0.2% and it increases with increasing of $< VB_s >$.

(4) HFAE and FE10k criteria events also occur at higher $< VB_s >$ magnitudes, up to 7 mV/m (with one event in 8-9 mV/m bin) and up to 10 mV/m, respectively. The risk for the HFAE criterion severe environment to happen is 0.02% $\pm$ 0.1% with no clear dependence on the $< VB_s >$ magnitude. For the FE10k criterion, the percentage is higher, 0.6% $\pm$ 0.18%, with no dependence on the $< VB_s >$ magnitude, either. Since $< VB_s >$ is computed based on IMF B_Z and V_{SW} values, the risks are higher than those for solar wind number density and comparable with those shown in Figures 2a and b.

3.3 Risks for severe environments for surface charging dependent on criteria definitions

As was shown in the sections above, the peaks in the number of severe environment events and the risks for these events to happen depend on how they are defined in four

Criterion/ Parameter (range)	Kp, 0–9	AE, 0– 2200 nT	SYM-H, 50 – -300 nT	IMF B_z, -20 – -10 nT	V_{sw}, 200 – 1100 km/s	N_{sw}, 0 – 45 cm^{-3}	$< VB_s >$, 0- 11 mV/m
PG5k	3–4 (1–8)	500–600 (100–1600)	0 – -50 (25 – -100)	0 – -4 (4 – -14)	400–700 (300–1000)	0–5 (0–15)	0–2 (0–5)
LFHE	4–5 (1–9)	700–800 (200-1400)	-25 – -50 (25 – -275)	-2 – -6 (6 – -16)	400–500 (300–800)	5–10 (0–35)	2–3 (0–6)
HFAE	3–5 (1–9)	600–700 (200–2100)	-25 – -50 (25 – -150)	-2 – -4 (2 – -10)	500–700 (400–1000)	0–5 (0–20)	1–2 (0–7)
FE10k	4–5(7) (2–9)	1000–1100 (500–2200)	-25 – -75 (25 – -250)	-4 – -6 (2 – -20)	400–700 (300–900)	0–5 (0–35)	1–4 (0–10)

Table 2. Peaks in number of events with corresponding parameter magnitude and range.

criteria. Tables 2 and 3 summarize the obtained results of the above analysis of Figures 1 and 2.

Table 2 demonstrates for each criterion at what bin of the observed parameter the maximum number of the severe environment events was reached, together with the range in brackets of the parameter values at which the events were detected. The first row in the Table 2 also contains the observed ranges for each parameter during the 1990-2005 period (orange curves in the bottom panels in Figures 1 and 2).

Table 3 shows, for each criterion, the maximum risk in percentage to detect a worst-case severe environment event with the corresponding value of the parameter at this risk together with yes (Y) or no (N) for the dependence of the risk on the parameter.

Let us determine, which parameter(s) can be considered as an indicator that a worst-case severe environment event would occur for each criterion. The PG5k is the only criterion which depends on the spacecraft potential, so it is supposed to be most relevant to surface charging events. It needs to be reminded that the majority of these events are in eclipse, so, they are with only the effect of plasma condition on spacecraft potential. This can lead to a very risky situation when the spacecraft is in eclipse and, for example, the values of V_sw are high.

Criterion/ Risk ± δ, % param. (D)	Kp	AE, nT	SYM-H, nT	IMF B_z, nT	V_{sw}, km/s	N_{sw}, cm^{-3}	$< VB_s >$, mV/m
PG5k	0.04 ± 0.008 4-5 (N)	0.2 ± 0.1 1100 (N)	0.04 ± 0.01 -75 (N)	0.04 ± 0.007 -4 (N)	0.1 ± 0.07 800 (Y)	0.026 ± 0.003 0 (N)	0.07 ± 0.04 4 (N)
LFHE	0.2 ± 0.05 6-7 (N)	0.2 ± 0.1 1100 (N)	0.14 ± 0.06 -150 (N)	0.4 ± 0.16 -14 (Y)	0.02 ± 0.003 700 (N)	0.18 ± 0.13 35 (Y)	0.5 ± 0.2 6 (Y)
HFAE	0.08 ± 0.02 5-6 (N)	1.0 ± 0.5 1400 (N)	0.13 ± 0.04 -100 (Y)	0.06 ± 0.02 -8 (N)	0.7 ± 0.4 900 (Y)	0.03 ± 0.003 0 (N)	0.2 ± 0.1 5 (N)
FE10k	0.5 ± 0.2 8-9 (Y)	2.3 ± 1.3 1700 (N)	0.3 ± 0.2 -175 (N)	0.46 ± 0.18 -14 (Y)	0.2 ± 0.1 800 (Y)	0.03 ± 0.007 10 (Y)	0.6 ± 0.18 8 (Y)

Table 3. Highest risk with corresponding uncertainty to detect a worst-case severe environment event at the corresponding value of the parameter and presence of a risk-parameter dependence.

For PG5k criterion:

(1) worst-case severe environments occur under slightly disturbed conditions (Kp = 3-4, moderate substorm activity of 500-600 nT, no storm activity, no significant IMF B_z, N_{sw}, VB_s) but with V_{sw} elevated to 700 km/s (Table 2);

(2) two parameters, AE and V_{sw}, can serve as indicators of the increased risk (maximum of 0.2% ± 0.1% at AE of 1100 nT and 0.1% ± 0.07% at V_{sw} of 800 km/s) for a worst-case severe environment event to occur and the risk for these events depends on the value of the parameters (Table 3).

The three other criteria are based on the fluxes and, therefore, are not directly related to the spacecraft potential. For the LFHE criterion:

(1) worst-case severe environments occur under moderately disturbed conditions (Kp = 4-5, moderate substorm activity of 700-800 nT, main phase of small storms, negative IMF B_z of -6 nT, no significant increase in V_{sw}) but elevated N_{sw} of 5-10 cm^{-3} and $< VB_s >$ of 2-3 mV/m (Table 2);

(2) the highest risks are associated with IMF B_z (0.4% ± 0.16% at -14 nT) and, as an effect, $< VB_s >$ (0.5% ± 0.2% at 6 mV/m) and the risks exhibit dependencies on the values of these two parameters (Table 3). The question mark for the IMF B_z dependence stresses that the last dot in Figure 2a, second panel, does not fit into the dependence. The third parameter, N_{sw}, though not with high risk percentage, influences the risk so that it increases with N_{sw} increase.

For the HFAE criterion:

(1) worst-case severe environments occur under moderately disturbed conditions (Kp = 3-5, moderate substorm activity of 600-700 nT, recovery phase of small storms, negative IMF B_z of -4 nT, no significant N_{sw} and $< VB_s >$) but with V_{sw} elevated to 700 km/s (Table 2);

(2) similarly to the PG5k criterion, two parameters, AE and V_{sw}, are related to the highest risks for a worst-case severe environment event to occur (1.0% ± 0.5% at 1400 nT and 0.7% ± 0.4% at 900 km/s), but only the risk associated with V_{sw} depends on its value. The third highest risk of 0.2% ± 0.1% is for $< VB_s >$ which follows from the high risk for V_{sw}.

For the FE10k criterion:

(1) worst-case severe environments occur under slightly more intensely disturbed conditions (Kp = 4-5(7), intense substorm activity of 1000-1100 nT, main and recovery phases of small to moderate storms, negative IMF B_z of -6 nT, no significant N_{sw}) but with V_{sw} elevated to 700 km/s and, as follows, VB_s of 2-3 mV/m (Table 2);

(2) all parameters (except of V_{sw} and N_{sw}) have higher risks, as compared with the other three criteria, and for all of them (except of AE and SYM-H) the associated risks show the dependencies of parameters' values.

Thus, to summarize:

(i) the range of geomagnetic conditions for maximum number of worst-case severe environments for surface charging to occur including all four criteria:

(a) moderately disturbed with Kp from 3 to 5;

(b) moderate to intense substorm activity with AE from 500 to 1000 nT;

(c) storm activity from none to main and recovery phases of small to moderate storms;

(d) slightly negative IMF B_z up to -6 nT;

(e) V_{sw} from 400 and elevated to 700 km/s;

(f) low N_{sw} with 5-10 cm^{-3} only for one criteria of LFHE;

(g) as follows from IMF B_z and V_{sw}, $< VB_s > < 4$ mV/m.

(ii) geomagnetic indices and IMF and solar wind parameters and their relations to the maximum risks for worst-case severe environments for surface charging to occur including all four criteria:

(a) Kp index is not associated with highest risk for worst-case severe environments to occur, the only criterion is FE10k for which the risk and the Kp value are related;

(b) AE index determines the highest/close to highest risk, except for the LFHE criterion, but the risk is not dependent on the AE magnitude;

(c) no high risk is related to the SYM-H index and there is no dependence on its value for the risk;

(d) elevated risks with not 100% clear dependencies exist for IMF B_z;

(e) V_{sw} directly indicates the highest risk for worst-case severe environments to happen and this risk depends on the V_{sw} value, except for the LFHE criteria;

(f) no high risk is associated with the N_{sw} but the risk depends on N_{sw} magnitude for the LFHE and FE10k criteria;

(g) the risks for $< VB_s >$ are determined by the risks for IMF B_z and V_{sw}.

AE and V_{sw} are the most important parameters which can define the occurrence of worst-case severe environments for surface charging.

4 Worst-Case Severe Environments for Surface Charging with Superimposed Epoch Analysis

In addition to studying the dependencies of severe environments for surface charging on current activity defined by geomagnetic indices (Figure 1) and one hour averaged IMF and solar wind parameters (Figure 2), we conducted the superimposed epoch analysis for all the detected events with four criteria. The observed index or IMF or solar wind parameter during an event was plotted a certain number of hours before and after the time of an event and all of the plots were combined setting the time of the events as zero for all of them. Such analysis helps to identify the general behaviour of the observed index or IMF or solar wind parameter before and after all events belonging to a specific criterion.

4.1 Geomagnetic Indices

Figure 3 demonstrates the results of the superimposed epoch analysis conducted for the variations of (a) Kp, (b) AE, (c) AL, and (d) SYM-H indices at around the detected top 100 15 minute-averaged worst-case severe environments for surface charging. As in previous Figures 1 and 2, top panel is for PG5k (purple), second panel is for LFHE (green), third panel is for HFAE (red), and bottom panel is for FE10k (blue) criteria. Each panel presents the median value for the corresponding index (thick line, bold squares for Kp) with the shaded area (bars for Kp) of the interquartile range (25th-75th percentile). In Figure 3a, for each event, the observed Kp values are plotted for every 3 hours for the interval of 24 hours before and 12 hours after an event for the four criteria. The Kp index does not change much before and after events in the PG5k and HFAE criteria. At the same time, the Kp values before and after events were not low: around 3 for a PG5k event and 4 for a HFAE event (as shown by median). Two other criteria, both flux related, show the increase in Kp index before and decrease after the event with the peak at the time of the event. For LFHE events, the Kp index starts to increase from low values of 2 to 3 about 9 hours before the event reaching about 4.5 at the time of the event with subsequent gradual decrease to 3 twelve hours after the event. The Kp index was somewhat elevated being between 3 and 4 during 24 to 6 hours before the event in the

FE10k criterion, reached about 5.3 and decreased to 4 in 12 hours after the event. These variations are not big; nevertheless, the pattern of Kp changes as seen in the superimposed epoch analysis confirm that the magnetosphere needs to be in an active state (Kp > 2) for an event to occur.

Figure 3b shows the observed 1 min AE values plotted 9 hours before and 6 hours after the event for four criteria. For all criteria, the AE index was elevated as compared to times before and after an event. For the spacecraft potential criterion PG5k, the AE was about 300-400 nT during 8 hours and then increased up to 600 nT during 1 hour before the event with gradual decrease back to about 300 nT (looking at median values). The AE index during LFHE events gradually increased from 200 nT 9 hours before the event reaching maximum values of 600 nT 1 hour before the event and starting to decrease right at the time of the event, also going gradually back to 300 nT 6 hours after the event.

The AE index during HFAE and FE10k criteria events shows the most sharp peaks. The AE index for HFAE events reached its peak of 800 nT during 1 hour before the event being about 400 nT during 8 preceding hours and returned to this value of 400 nT in 2 hours after the event. The AE index for FE10k events started to increase from 400 nT magnitudes 5 hours before the event with the peak value of 1000 nT at the time of the event and decreased in 3 hours to 500 nT.

The AE index (Davis & Sugiura, 1966) was developed to reflect the strength of ionospheric currents flowing in the auroral oval during substorms. The AE index is the difference between the AU (auroral upper) index, which measures the strength of the eastward electrojet flowing from mid-afternoon toward midnight, and the AL (auroral lower) index which measures the strength of the westward electrojet that flows from dawn to past midnight. The AL component of AE is especially useful for substorm studies, since it is sensitive to the ionospheric currents that flow through the auroral bulge during the expansion phase (Akasofu et al., 1965). Therefore, in addition to the AE index, we show also the variations of the AL index in the present study. Figure 3c shows the observed 1 min AL values, similarly to Figure 3b. For the AE index, the events in all four criteria occur when the AL index has its peaks (minima in this case). The most sharp and deep minima in AL are seen again for HFAE and FE10k criteria events, -600 nT and -750 nT in median, respectively. The behavior of AL is very similar as to AE before and

after the events. The most gradual decrease before the event and recovery after the event is again evident for LFHE events: the minimum of -450 nT is reached 1 hour before the event and the recovery starts right at the event. The AL index during PG5k events exhibits a pattern very similar to the one for the AE index.

In Figure 3d, 1 min SYM-H values are plotted 24 hours (1 day) before and 72 hours (3 days) after the event for four criteria. The behavior of the SYM-H index is similar to that of the Kp index in such a way that no significant changes exist in the SYM-H index as seen in the median lines during PG5k and HFAE events but SYM-H variations are present for LFHE and FE10k criteria events (see Figure 3a for comparison). During PG5k events, the median SYM-H index is about -20 nT 1 day before and 3 days after the event with slight decrease to -25 nT at the time of the event. The median SYM-H during HFAE events does not show any dips before or after the event but SYM-H is -40 nT 1 day before the event and as can be seen in the interquartile range, SYM-H can reach -60 nT and stay like that 1 days before the event gradually increasing to -40 nT after. The only criterion for an event to happen when SYM-H is minimal and the whole pattern of the SYM-H corresponds to a storm time one is the LFHE criteria. SYM-H being about -15 nT in median 1 day before the event, starts to decrease sharply 4 hours before the event. LFHE events occur during rather moderate SYM-H values, no lower than -60 nT in minimum. In 3 days, the SYM-H index recovers back to -20 nT. During FE10k events, the SYM-H index also decreases before the event but more gradually than during LFHE events. The event occurs right before the SYM-H minimum, not at the minimum. The minimum SYM-H value can be as low as -90 nT within 8 hours after the event according to the interquartile range. It should be noted that out of all indices, only AE and AL demonstrate clear variation for a PG5k event (PG5k is the only criterion connected to spacecraft potential).

4.2 IMF and Solar Wind Parameters

Similarly to Figure 3, Figure 4 demonstrates the results of the superimposed epoch analysis conducted for the variations of (a) IMF B_Z, (b) solar wind speed V_{SW}, (c) number density N_{SW}, and (d) E_y electric field at around the detected top 100 15 minute-averaged worst-case severe environments for surface charging. In the superposed epoch analysis, we use E_y instead of $<VB_s>$, since the latter one is proportional to the integral (over 1 hour prior to the epoch zero) of the former with zeroed values correspond-

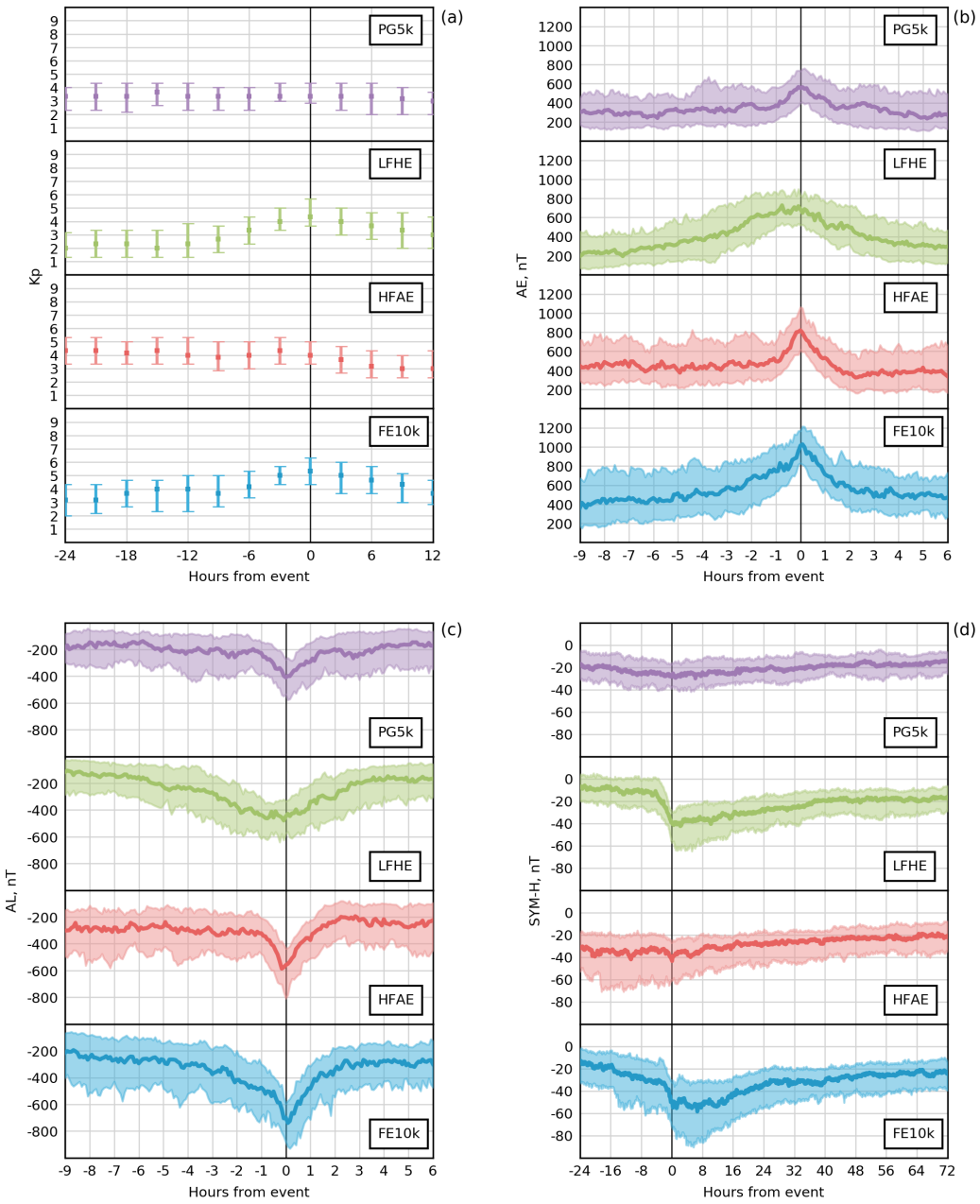

Figure 3. Superimposed epoch analysis for the variations of (a) Kp, (b) AE, (c) AL, and (d) SYM-H indices at around the detected top 100 15 minute-averaged worst-case severe environments for surface charging. Thick lines represent the median index value at each 1 min time step (bold squares for median Kp value at each 3-hour time step) and shaded area (bars for Kp index) defines the interquartile range (25th-75th percentile).

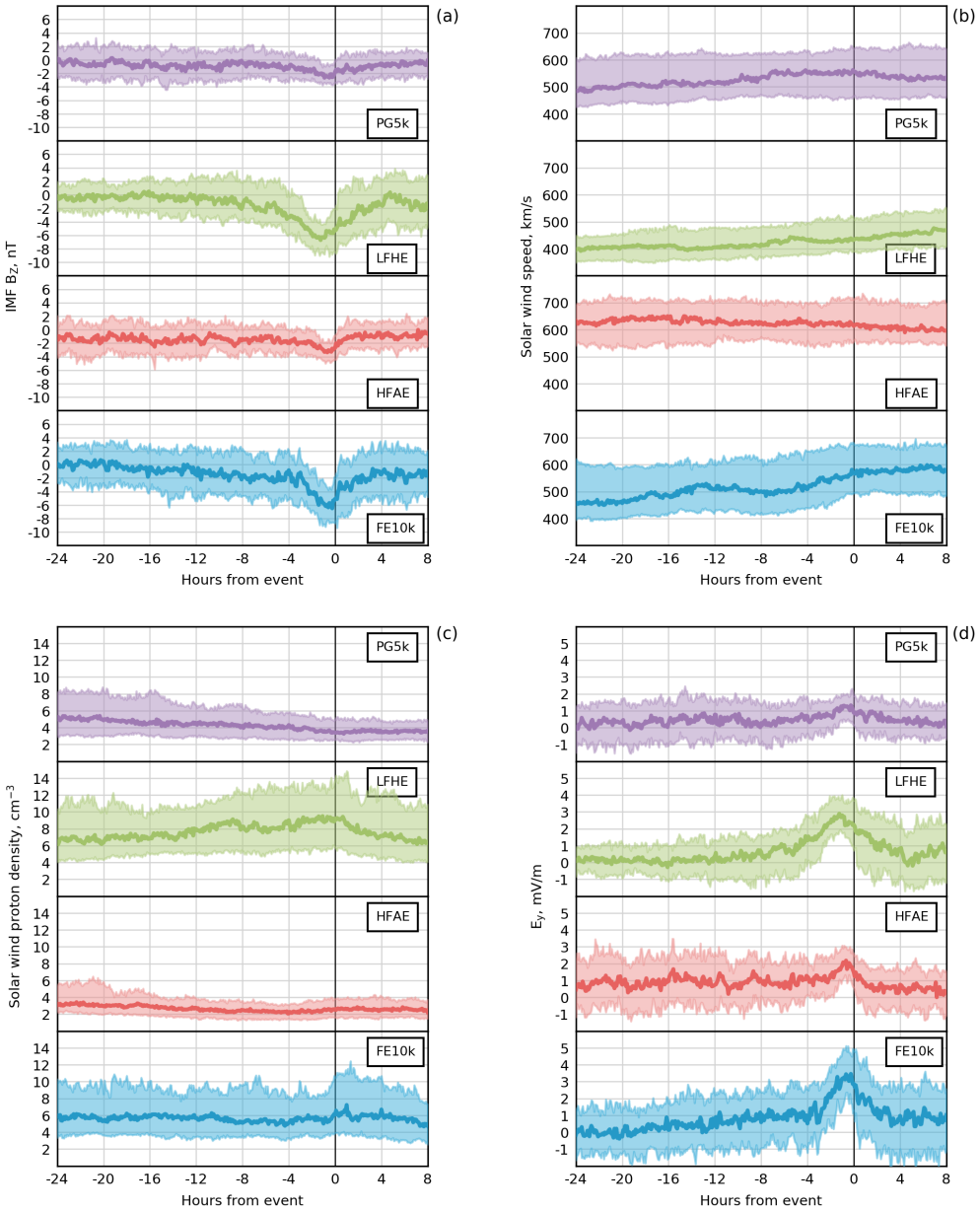

Figure 4. Similarly to Figure 3, superimposed epoch analysis for the variations of (a) IMF B_Z, (b) solar wind velocity, (c) number density, and (d) E_y electric field at around the detected top 100 15 minute-averaged worst-case severe environments for surface charging. Thick lines represent the median values at each 1 min time step and shaded area defines the interquartile range (25th-75th percentile).

ing to positive IMF B_Z measurements. Thick lines represent the median values at each 5 min time step and shaded area defines the interquartile range (25th-75th percentile).

In Figure 4a, for each event, the observed 5 minute IMF B_Z values are plotted for the interval of 24 hours before and 8 hours after an event for four criteria. As can be seen, the most pronounced changes in the IMF B_Z behavior before and after the event are for LFHE and FE10k criteria events, while changes are not so big for PG5k and HFAE events. During all events, IMF B_Z exhibits a minimum but the occurrence of this minimum does not coincide with the time of the event, being always before the event. The delay is 1-2 h which is around a typical substorm growth phase timescale.

For the LFHE criterion, the IMF B_Z stays at about 0 nT in median from 24 to 8 hours before the event, then starts to decrease, reaching its minimum of about -6 nT 1.5 hours before the event. IMF B_Z recovers to zero by the 5th hour after the event but then drops to -2 nT. During the recovery, the range of interquartiles is wider than before the event, being -2 to 2 nT from the median. IMF B_Z during the FE10k criterion events show very similar time-dependence: it decreased slowly to -2 nT from 12 to 4 hours before the event and then dropped faster to -6 nT at about 1 hour before the event. It comes back to about -1 nT 4 hours after the event. During PG5k and HFAE events, IMF B_Z decreases before and increases after the event but the change is not larger than 1 nT.

Figure 4b presents the observed 5 minute V_{SW} values plotted for the interval of 24 hours before and 8 hours after an event for the four criteria. No sharp variations in V_{SW} can be seen before and after the events in all four criteria, but V_{SW} is noticeably higher than the average solar wind velocity ($\sim$400km/s) for all but LFHE criteria. For events in the PG5k criterion, V_{SW} is at about 500 km/s from 24 to 8 hours before the event and then increases to 550 km/s and stays at that value. For events in the LFHE criterion, again from 24 to 8 hours before the event, V_{SW} is at 400 km/s and then gradually increases to 470 km/s by the 8th hour after the event. V_{SW} magnitudes are the highest for HFAE events, being 600-650 km/s throughout all the time interval. FE10k criterion events correspond to the largest, though smoothest changes in V_{SW} before and after the event: from 460 to 600 km/s.

Similarly to Figures 4a and 4b, Figure 4c shows the observed 5 minute N_{SW} values for the four criteria. As in case of V_{SW}, PG5k and HFAE events are not associated with changes in N_{SW}: N_{SW} is about 4-5 cm^{-3} for PG5k and about 3 cm^{-3} for HFAE

criteria as seen in the median values. The interquartile range in N_{SW} is wider for the PG5k criterion 24 hours before the event (3-8 cm^{-3}) and then narrows down to ± 1 from the median value at the event and 8 hours after. For LFHE events, N_{SW} is elevated to 7 cm^{-3} during 24 to 14 hours before the event, then starts to increase gradually, reaches 9 cm^{-3} at the event, and decreases to 6 cm^{-3} 8 hours after the event. The interquartile range is wider than for PG5k and HFAE events being 6-14 cm^{-3} at the event. In any case, there are no sharp variations in N_{SW}. During FE10k events, N_{SW} changes are also small, N_{SW} stays at 6 cm^{-3} from 24 hours right up to 1 hour before the event, then increases slightly and comes back to the initial value.

Variations of the derived E_y presented in Figure 4d reflect very much of the variations in IMF B_Z seen in Figure 4a. For all criteria, E_y has a peak right at about 1 hour before the event. The smallest peak is observed during PG5k events, the sharpest - during FE10k events. Monotonic increase of E_y from 0 to 1 mV/m until 3 hours before the event, then increase to about 3.5 mV/m in 2 hours and subsequent decrease back to initial magnitudes are typical characteristics of FE10k events. The interquartile range is 2-5 mV/m. During LFHE events, E_y stays at around 0 until about 8 hours before the event, then starts to increase more gradually than during FE10k events and reaches a peak median value of 3 mV/m. The E_y goes back to 0 values after the peak until 5 hours after the event and then increases up to 1 mV/m. HFAE events correspond to a smaller peak in E_y: E_y oscillates around 1 mV/m until about 2 hours before the event and then increases by only 1 mV/m recovering in 3 hours back to initial magnitudes. During PG5k events, the changes in E_y are very small: the E_y values lie between 0 and 1 mV/m and increase only up to 1.5 mV/m 1 hour before the event.

4.3 Time history for severe environments for surface charging dependent on criteria definitions

Similarly to the results presented in previous sections, the time history of the parameters before, at and after the events of severe environments for surface charging differs for different criteria definitions. Table 4 summarized the noticeable parameter changes over time before the event (for example, there is a 300 nT change in AE during 1 hour before the event), the time when the maximal change (maximum or minimum) in the parameter occur relative to the time of the event (for example, the AE peaks at the time of the event), and how many hours it takes for the parameter to recover to its initial mag-

Criterion/ Parameter	ΔKp	ΔAE, nT	ΔAL, nT	ΔSYM-H, nT	ΔIMF B_z, nT	ΔV_{sw}, km/s	ΔN_{sw}, cm^{-3}	Δ$< VB_s >$, mV/m
PG5k	No	300 in 1h/ max at/ 4h	200 in 1.5h/ max at/ 1.5h	No	No (2 1h before)	No	No	1 in 8h/ max 1h before/4h
LFHE	2 in 9h/ max at/ 12h	600 in 8h/ max 1h before/ 6h	230 in 6h/ max 0.5h before/3h	30 in 4h/ max at/ 36h	6 in 8h/ max 1h before/5h	50 grad. inc.	3 grad. inc./ decr.	3 in 8h/ max 1.5h before/4h
HFAE	No	400 in 1h/ max at/ 2h	300 in 1h/ max 20 min before/2h	No	No (2 1h before)	No	No	1 in 2h/ max 1h before/2h
FE10k	2 in 6h/ max at/ 12h	600 in 5h/ max at/ 3h	450 in 5h/ max at/ 2h	50 in 24h/ max 4h after/>40h	6 in 4h/ max 1h before/4h	100 grad. incr.	No	3 in 4h/ max 1h before/4h

Table 4. Parameter changes with time before the event/relative timing of parameter maximum change and the even/and after the event

nitude (for example, it take about 4 hours for AE to recover) for the four criteria. All numbers refer to the median values seen in Figures 3 and 4.

For the PG5k criterion based on the spacecraft potential, no changes are seen in the Kp and SYM-H indices, solar wind velocity and number density. IMF B_z exhibits a small, rather questionable change of 2 nT during 1 hour before the event and, as a consequence, E_y shows 1 mV/m change in 8 hours before the event. The only noticeable change is in AE (and AL) with 300 nT in 1 hour before the event (200 nT in 1.5 hours for AL), and the peak in AE (and minimum drop in AL) occurred at the time of the event with fast recovery.

For the flux based LFHE criterion, all parameters change but on a longer time period, more than in 1 hour before the event as seen in the PG5k criterion. The Kp index increases from 2 to 4 in 9 hours before the event, reaching its maximum at the time of the event and slowly recovering in 12 hours. AE (600 nT in 8 hours) and AL (230 nT

in 6 hours) show gradual changes with no distinct peaks. The maximal change occurs 0.5-1 hour before the event. Even more gradual changes are seen for V_{sw} (only 50 km7s change) and N_{sw}. Sharp changes are present in SYM-H (30 nT in 4 hours with maximum at the event with long recovery) but they are not large. IMF B_z drops from 0 to -6 nT in 8 hours reaching minimum of -6 nT 1 hour before the event and so E_y has a peak 1.5 hours before the event with 3 mV/m change from 0 in 8 hours.

Behaviour of the parameters during HFAE events is rather similar to the PG5k criterion. No changes can be seen for Kp and SYM-H indices, solar wind velocity and number density with small changes in IMF B_z and VB_s. Again, the only parameters with significant changes are AE and AL. They exhibit sharp changes of 300-400 nT in 1 hour before the event with maximum change at the time of the event (20 minutes shift for AL) with fast recovery of 2 hours.

Events with the last criterion, FE10k, are associated with significant changes in all parameters, except for V_{sw} and N_{sw}. Kp changes by 2 in 6 hours, AE increases by 600 nT in 5 hours, AE drops by 450 nT in 5 hours and they all have their maximal change at the time of the event. SYM-H shows a rather gradual decrease of 50 nT in 24 hours with maximal drop 4 hours after the event and long recovery. IMF B_z and E_y change by 6 nT and 3 mV/m, respectively, in 4 hours reaching maximal change 1 hour before the event.

Thus, based on the significance and timing of changes in the parameters before and at the events of severe environments for surface charging for different criteria definitions, we can summarize as follows:

(a) No changes are seen in V_{sw} and N_{sw} for all four criteria;

(b) A substorm-type pattern of the superimposed epoch AE (AL) dependencies for all criteria: 300-600 nT changes in AE (AL) are associated with the events for all four criteria with maximum change coinciding with the time of the event (gradual changes with maximum 1 hour before the event for LFHE events);

(c) A storm-type pattern of the superimposed epoch SYM-H dependencies for LFHE and FE10k criteria, not for PG5k and HFAE criteria: 30 nT sharp drop at the event for LFHE and gradual 50 nT drop 4 hours after the event for FE10k;

(d) The Kp index starts to increase 6-9 hours before the event with the change of about 2 reaching maximum at the time of the event for 2 (LFHE and FE10k) out of 4 criteria;

(e) Southward turning in IMF B_z: for LFHE and FE10k events, IMF B_z starts to decrease from being 0 and reaches maximum drop of 6 nT in 4-8 hours at 1 hour before the event occurring. Small changes of no more than 2 nT with maximum at 1 hour before the event are seen for PG5k and HFAE events. Corresponding changes are evident in E_y.

AE and IMF B_z are the parameters with the most definite changes before and at the time of the events of worst-case severe environments for surface charging.

5 Discussion and Conclusions

The occurrences of 400 worst-case severe environments for surface charging observed by LANL satellites during the years of 1990-2005 were analyzed based on the definitions of four criteria for the worst-case severe environments developed by Matéo-Vélez et al. (2018) and the activity parameters with their time history, such as Kp, AE, AL, and SYM-H indices and IMF B_Z, solar wind speed, proton number density, and derived electric field E_y and $<VB_s>$. In addition to the occurrences (or numbers of events as histograms in Figures 1 and 2) of worst case severe environments, the normalized severe environment occurrence rate was introduced (shown as black dots with uncertainties in Figures 1 and 2). These normalized occurrence rates are the indicators of a risk to detect a top 100 worst-case severe environment event in a 15 min window for a given parameter bin.

For the Kp index to be considered as the main indicator of the probability for a satellite anomaly to be detected, no Kp-dependent high risk for worst-case severe environments for surface charging was found. During all events, the magnetosphere was moderately disturbed with Kp ranging from 3 to 5. This is in agreement with the previous studies by, for example, Choi et al. (2011); Thomsen et al. (2013); Matéo-Vélez et al. (2018); Matéo-Vélez et al. (2019), (more citations can be found in the Introduction section) where it was stated that rather moderate Kp values were observed during the charging events. Charging events do not necessarily require high values of Kp.

The AE index was found to be a very special indicator of the highest risk for severe environments for surface charging to happen. Before and after the events in all cri-

teria, the AE (AL) index shows a substorm-type pattern with max/min at the time of the event. This is in agreement with many previous studies relating the observed spacecraft anomalies with the presence of substorm activity. For example, Saiz et al. (2018) found that during the loss of Telstar 401 on 11 January 1997, the Kp index reached only 4, but a substorm occurred about 45 min before the anomaly (similarly to LFHE criteria). Iucci et al. (2005, 2006) have developed and analyzed the database of anomalies from Russian Kosmos satellites which occurred during 19711997. Based on the dependence on the local time and AE index, they concluded that local-time dependent anomalies were due to 10-15 keV electrons injected into the magnetosphere as a result of auroral substorms. Loto'aniu et al. (2015) analyzed the space weather conditions at and around the time of the widely-studied anomaly (Allen, 2010) at geosynchronous Galaxy 15 spacecraft at local midnight and concluded that the attributed onboard electrostatic discharge was due to the interactions of the spacecraft with substorm-injected energetic particles leading to spacecraft charging. At the same time, our analysis shows that the risk for severe environments for surface charging does not depend on the AE magnitude. The presence of substorm activity can tell us that the environment can be severe for surface charging to occur, but the surface charging will not depend on whether a substorm was moderate or intense.

Storm-type patterns of the SYM-H behavior during the events with LFHE and FE10k criteria based on low energy fluxes were obtained, but no high risk and no dependence on the strength of a storm were found related to the SYM-H index. Not many studies have attempted to relate the Dst index with the observed anomalies. One of them by Lohmeyer et al. (2012) correlated Inmarsat anomalies with only a -25 nT drop in the Dst index. Most of the events in the present study which had relations to the SYM-H index occurred during main and recovery phases of small to moderate storms with SYM-H above -100 nT. At the same time, many events occurred without any relation to any storm. Thus, there is no need for a storm of any strength to happen in order for a surface charging event to be detected.

If the detection of a severe environment for surface charging requires ongoing substorm activity, then AE (AL) index, but not Kp or SYM-H (Dst), is naturally best suited to characterize this environment. Related to that, it is also quite expected that superimposed epoch IMF B_z revealed the southward turning pattern 1 hour before the events. The IMF B_z itself cannot serve as an indicator of a risk to have a severe environment.

Sillanpää et al. (2017) conducted the analysis of GOES 13 MAGED data for 5 years (20112015) and developed an empirical model for the 40-150 keV electron fluxes at geostationary orbit. They found that 1.5h delayed IMF B_Z and V_{sw} are the driving parameters for the best correlation between the modeled and observed electron fluxes. Ganushkina et al. (2019) further confirmed this. Indeed, according to our present study, V_{sw} is related to the highest risk worst-case severe environments and this risk depends on the V_{sw} magnitude. The difference is that the time history of V_{sw} before and after the events in all four criteria for worst-case severe environments does not contain any significant variations. The event of worst-case severe environment is not related to V_{sw} sharp changes but it occurs when V_{sw} is elevated to 500-700 km/s for prolonged periods.

Saiz et al. (2018) reported that in the case of Telstar 401 anomaly, the most important parameters were large (>10 nT) fluctuations of IMF B_y and high solar wind dynamic pressure (reaching 50 nPa). We included N_{sw} in the list of the studied parameters and found no risk associated with it and no changes in the time history of it.

Our last parameter is $<VB_s>$, which has been used in modelling of low energy electron fluxes. For example, Denton et al. (2016) introduced the empirical model of the electron fluxes and ion fluxes at geosynchronous orbit as a function of local time, energy, and $<VB_s>$. Stepanov et al. (2021) used THEMIS (The Time History of Events and Macroscale Interactions during Substorms) dataset to investigated a relative importance of the various external driving parameters for the superthermal electron flux variations. The authors ranked solar wind reconnection electric field Ekl ($Ekl = VB_{yz}sin^2(\theta/2)$) as the second (in its importance, after V_{sw}) parameter controlling 10 keV electron flux. Obviously, $<VB_s>$ defines the risks for worst-case severe environments according to those of IMF B_z and V_{sw}.

Among four criteria for surface charging related, severe environments developed by Matéo-Vélez et al. (2018), LFHE and FE10k criteria based on the enhancements of low energy particle fluxes show definitely clearer dependencies on the solar wind and IMF parameters and geomagnetic activity indices and distinct variations in the superimposed epoch patterns. LFHE is regarded as high fluxes of electrons with energies < 50 keV and low fluxes for electrons with energies > 200 keV. FE10k is related to the highest fluxes of electrons at energies above 10 keV. Low energy electrons vary significantly with the geomagnetic conditions (e.g., Ganushkina et al., 2013; Sillanpää et al., 2017; Ganushk-

ina et al., 2019). Therefore, there is no surprise that the occurrence of severe environment events classified as those two criteria exhibits more pronounced dependencies on the solar wind and IMF parameters and geomagnetic activity indices. At the same time, the similar dependencies are less obvious for the PG5k criterion based on spacecraft potential stressing again the absence of straightforward relations between the geomagnetic conditions and surface charging.

On the other hand, PG5k criterion is based on the duration of charging even though below extreme value (in contrast to other criteria which are based on peak values). It can be speculated that this specific feature could lead to the some kind of saturation seen in some figures (e.g. Figure 1a, b). If it is the case, the beginning of saturation corresponds to -5 kV charging. In addition, since almost all top 100 PG5k events occurred in eclipse and LANL spacecraft spend relatively little time in eclipse, the events with extreme geomagnetical activity can be represented poorly in the dataset. This could possibly make the dependence on activity less clear. It should be noted that absolute charging is different from differential charging. High absolute charging levels make charging risks higher but only if they are associated with high differential voltages. Too few spacecraft are equipped with sensors to allow assessing both at the same time. In the present study, we have looked at long duration charging events that could possibly lead also to high differential charging (PG5k) and on electron spectra that can produce both absolute and differential charging on the basis of particle-matter interactions.

In reality, there were many more events with severe environments detected by LANL satellites during 1990-2005 (Matéo-Vélez et al., 2018). One of the logical steps in continuation of the presented study would be an analysis using all data with a parameter above a given threshold. Such a threshold could be a potential below -100 V, or a flux of $>$ 10 kev electrons above $10^7\ cm^{-2}\ sec^{-1}\ sr^{-1}\ keV^{-1}$, etc. This analysis can verify the obtained conclusions.

Another useful study will be to perform similar as in the present study analysis by separating events outside and inside eclipse to get the events in PG5k criterion in eclipse and the events in PGXk criterion outside eclipse with X being a potential to be determined. For the Van Allen Probes data analysis, Matéo-Vélez et al. (2019) have used -100 V for potential X. Criteria based on satellite potential could distinguish events with a potential exceeding a given potential (as e.g. -100 V). In addition, sorting out events

inside and outside eclipse would help to separate better the effect of photoemission from ambient plasma and geomagnetic conditions.

Keeping in mind the points discussed above, the conclusions are the followings:

1. Moderate to intense substorm activity with the AE index ranging from about 500 to 1000 nT is present when severe environments are detected and time history of AE (AL) before and after events in all criteria exhibits a substorm-type pattern with max/min at the time of the event. The AE index determines the highest risk for severe environments for surface charging to happen, but this risk does not depend on the AE magnitude.

2. V_{sw} points directly to the highest risk dependent on the V_{sw} value to worst-case severe environments to happen. At the same time, no significant changes were seen in the time history of V_{sw} before and after the events in all four criteria, although V_{sw} values are elevated to 700 km/s for HFAE criterion.

3. Although no high risks for severe environments to occur related to the SYM-H index were found, a storm-type pattern of the superimposed epoch SYM-H for LFHE and FE10k low energy fluxes criteria was obtained, but the events were associated with main and recovery phases of small to moderate storms.

4. Worst-case severe environments for surface charging according to all four criteria occur when the Kp index shows moderate disturbance (3 to 5) but a high risk for them is not associated with the Kp index; changes in Kp index as increase in 6-9 hours exist only before events defined by LFHE and FE10k criteria which are based on high fluxes of low energy electrons.

5. IMF B_z was found to be small and negative during the events in all criteria with superimposed epoch analysis revealing the southward turning pattern in IMF B_z for LFHE and FE10k events with maximum drop of -6 nT one hour before the event occurring and smaller changes for PG5k and HFAE events. There is no clear dependence of risk to have a severe environment on IMF B_z.

6. As expected, the risks and time history for VB_s are determined by the risks and time history for IMF B_z and V_{sw}.

7. N_{sw} was $<5\ cm^{-3}$ for all criteria except for LFHE when it was 2 times higher. No high risk was found to be associated with the N_{sw} but there exists a dependence on

the N_{sw} magnitude for LFHE and FE10k criteria. No changes were seen in the time history of N_{sw}.

The conducted analysis demonstrated that events detected following two criteria, LFHE and FE10k, based on the enhancements of low energy particle fluxes are evidently different from other two (PG5k and HFAE) with larger magnitudes of the parameters and distinct patterns in the time history of them. It is necessary to stress that flux criteria are more easily generalized to non-LANL spacecraft whilst PG5k is uniquely determined by spacecraft materials, designs, and geometries.

Acknowledgments

The work at the University of Michigan was partly funded by National Aeronautics and Space Administration grants NNX17AI48G, 80NSSC20K0353, NNX17AB87G, and 80NSSC20K1504, and National Science Foundation grant 1663770. The contributions by N. Ganushkina and S. Dubyagin were also partly supported by the framework of the Finnish Centre of Excellence in Research of Sustainable Space (Academy of Finland decisions 312351 and 312390), by the Academy of Finland (grant 339329), and by the ESA Contract No 4000128226/19/NL/AS "Plasma Environment Modelling in the Earths Magnetosphere". For solar wind and IMF data, OMNIWeb (http://omniweb.gsfc.nasa.gov/) was used and geomagnetic indices were obtained from the World Data Center for Geomagnetism, Kyoto (http://wdc.kugi.kyoto-u.ac.jp/wdc/Sec3.html). 400 events with dates and times of the worst-case severe environments for surface charging as observed by LANL satellites during the years of 1990-2005 can be found at http://doi.org/10.5281/zenodo.4474594. They have been made through CNES Research and Technology Program funding 2016-2017.

References

Akasofu, S. I., Chapman, S., & Meng, C. I. (1965). The polar electrojet. *Journal of Atmospheric and Solar-Terrestrial Physics*, *27*(11/12), 1275 1305. doi: 10.1016/0021-9169(65)90087-5

Allen, J. (2010). The galaxy 15 anomaly: Another satellite in the wrong place at a critical time. *Space Weather*, *8*(6). doi: 10.1029/2010SW000588

Bame, S. J., McComas, D. J., Thomsen, M. F., Barraclough, B. L., Elphic, R. C., Glore, J. P., ... Wymer, F. J. (1993). Magnetospheric plasma analyzer for spacecraft with constrained resources. *Review of Scientific Instruments*, *64*(4),

1026-1033. doi: 10.1063/1.1144173

Belian, R. D., Gisler, G. R., Cayton, T., & Christensen, R. (1992). High-Z energetic particles at geosynchronous orbit during the Great Solar Proton Event Series of October 1989. *Journal of Geophysical Research: Space Physics*, *97*(A11), 16897-16906. doi: 10.1029/92JA01139

Bodeau, M. (2015). Review of better space weather proxies for spacecraft surface charging. *IEEE Transactions on Plasma Science*, *43*(9), 3075-3085. doi: 10.1109/TPS.2015.2441038

Choi, H. S., Lee, J., Cho, K. S., Kwak, Y. S., Cho, I. H., Park, Y. D., ... Lee, D. K. (2011). Analysis of GEO spacecraft anomalies: Space weather relationships. *Sp. Weather*, *9*(5), 1–12. doi: 10.1029/2010SW000597

Davis, T. N., & Sugiura, M. (1966). Auroral electrojet activity index ae and its universal time variations. *Journal of Geophysical Research (1896-1977)*, *71*(3), 785-801. doi: 10.1029/JZ071i003p00785

DeForest, S. E. (1972). Spacecraft charging at synchronous orbit. *J. Geophys. Res.*, *77*(4), 651–659. doi: 10.1029/JA077i004p00651

Denton, M. H., & Borovsky, J. E. (2012). Magnetosphere response to high-speed solar wind streams: A comparison of weak and strong driving and the importance of extended periods of fast solar wind. *Journal of Geophysical Research: Space Physics*, *117*(A9). doi: 10.1029/2011JA017124

Denton, M. H., Henderson, M. G., Jordanova, V. K., Thomsen, M. F., Borovsky, J. E., Woodroffe, J., ... Pitchford, D. (2016). An improved empirical model of electron and ion fluxes at geosynchronous orbit based on upstream solar wind conditions. *Space Weather*, *14*(7), 511-523. doi: 10.1002/2016SW001409

Farthing, W. H., Brown, J. P., & Bryant, W. C. (1982). *Differential Spacecraft Charging on the Geostationary Operational Environment Satellites* (Tech. Rep.). Greenbelt, Maryland. Retrieved from `https://ntrs.nasa.gov/search.jsp?R=19820018480`

Fennell, J. F., Koons, H. C., Roeder, J. L., & Blake, J. B. (2001). *Spacecraft charging: Observations and Relationship to Satellite Anomalies* (Tech. Rep.).

Ferguson, D., Hilmer, R., & Davis, V. (2015). Best Geosyncronous Earth Orbit Daytime Scpacecraft Charging Index. *J. Spacecr. Rockets*, *52*(2). doi: 10.2514/1.A32959

Fredricks, R. W., & Scarf, F. L. (1973). Observations of spacecraft charging effects in energetic plasma regions. In *Photon and particle interactions with surfaces in space* (pp. 277–308). Dordrecht, The Netherlands: Reidel.

Ganushkina, N. Y., Amariutei, O. A., Shprits, Y. Y., & Liemohn, M. W. (2013). Transport of the plasma sheet electrons to the geostationary distances. *Journal of Geophysical Research: Space Physics*, *118*(1), 82-98. doi: 10.1029/2012JA017923

Ganushkina, N. Y., Sillanp, I., Welling, D., Haiducek, J., Liemohn, M., Dubyagin, S., & Rodriguez, J. V. (2019). Validation of inner magnetosphere particle transport and acceleration model (imptam) with long-term goes maged measurements of kev electron fluxes at geostationary orbit. *Space Weather*, *17*(5), 687-708. doi: https://doi.org/10.1029/2018SW002028

Garrett, H. B. (1981). The charging of spacecraft surfaces. *Reviews of Geophysics*, *19*(4), 577-616. doi: 10.1029/RG019i004p00577

Grafodatskiy, O. S., Degtyarev, V. I., Kozlov, A. G., Lazarev, V. I., Platonov, O. I., Popov, G. V., & Teltsov, M. V. (1987). Relationship between characteristics of low-energy electrons and geo-magnetic disturbance in geostationary orbit. *Geomagnetism and Aeronomy*, *27*, 494-496.

Green, J. C., Likar, J., & Shprits, Y. (2017). Impact of space weather on the satellite industry. *Space Weather*, *15*(6), 804-818. doi: 10.1002/2017SW001646

Gubby, R., & Evans, J. (2002, 11). Space environment effects and satellite design. *Journal of Atmospheric and Solar-Terrestrial Physics*, *64*, 1723-1733. doi: 10.1016/S1364-6826(02)00122-0

Hastings, D., & Garrett, H. B. (1996). *Spacecraft-environment interactions.* Cambridge Univ. Press, New York.

Hoeber, C. F., Robertson, E. A., Katz, I., Davis, V. A., & Snyder, D. B. (1998). *Solar array augmented electrostatic discharge in geo* (Vol. AIAA 98-1401). Yokohama, Japan.

Huang, J., Liu, G., Jiang, L., & Yang, Y. (2017). Theory for geosynchronous spacecraft charging index. *Space Weather*, *15*(9), 1203-1211. doi: 10.1002/2017SW001670

Iucci, N., Dorman, L., Levitin, A., Belov, A., Eroshenko, E., Ptitsyna, N., ... Yanke, V. (2006). Spacecraft operational anomalies and space weather

impact hazards. *Advances in Space Research*, *37*(1), 184 - 190. doi: https://doi.org/10.1016/j.asr.2005.03.028

Iucci, N., Levitin, A. E., Belov, A. V., Eroshenko, E. A., Ptitsyna, N. G., Villoresi, G., ... G., Y. V. (2005). Space weather conditions and spacecraft anomalies in different orbits. *Space Weather*, *3*, S01001. doi: doi:10.1029/2003SW000056

Koons, H. C., & Gorney, D. J. (1991). Relationship Between Electrostatic Discharges on Spacecraft P78-2 and the Electron Environment. *Journal of Spacecraft and Rockets*, *28*(6), 683–688. doi: 10.2514/3.26300

Koons, H. C., Mazur, J., Lopatin, A., Pitchford, D., Bogorad, A., & Herschitz, R. (2006). Spatial and temporal correlation of spacecraft surface charging in geosynchronous orbit. *Journal of Spacecraft and Rockets*, *43*(1), 178-185. doi: 10.2514/1.10805

Koons, H. C., Mazur, J. E., Selesnick, R. S., Blake, J. B., Fennell, J. F., Roeder, J. L., & Anderson, P. C. (1999). The impact of the space environment on space systems. *Aerosp. Rep.*(September), 7–11. doi: 10.1017/CBO9781107415324.004

Koons, H. C., Mazur, J. E., Selesnick, R. S., Blake, J. B., Fennell, J. F., Roeder, J. L., & Anderson, P. C. (2000). *The impact of the space environment on space systems* (Vol. AFRL-VS-TR-20001578).

Lai, S. T., & Della-Rose, D. J. (2001). Spacecraft charging at geosynchronous altitudes: New evidence of existence of critical temperature. *Journal of Spacecraft and Rockets*, *38*(6), 922-928. doi: 10.2514/2.3764

Lai, S. T., Gussenhoven, M. S., & Cohen, H. A. (1983). *The concepts of critical temperature and energy cutoff of ambient electrons in high voltage charging of spacecraft.* European Space Agency, Noordwijk, Netherlands.

Lai, S. T., & Tautz, M. (2006). High-level spacecraft charging in eclipse at geosynchronous altitudes: A statistical study. *Journal of Geophysical Research: Space Physics*, *111*(A9). doi: 10.1029/2004JA010733

Lam, H.-L., Boteler, D. H., Burlton, B., & Evans, J. (2012). Anik-e1 and e2 satellite failures of january 1994 revisited. *Space Weather*, *10*(10). doi: 10.1029/2012SW000811

Lanzerotti, L., Breglia, C., Maurer, D., Johnson, G., & Maclennan, C. (1998, jan). Studies of spacecraft charging on a geosynchronous telecommunications satel-

lite. *Adv. Sp. Res.*, *22*(1), 79–82. doi: 10.1016/S0273-1177(97)01104-6

Lohmeyer, W., & Cahoy, K. (2013). Space weather radiation effects on geostationary satellite solid-state power amplifiers. *Space Weather*, *11*(8), 476-488. doi: 10.1002/swe.20071

Lohmeyer, W., Cahoy, K., & Baker, D. (2012). Correlation of geo communications satellite anomalies and space weather phenomena: Improved satellite performance and risk mitigation. In *30th aiaa international communications satellite system conference (icssc).* doi: 10.2514/6.2012-15083

Loto'aniu, T. M., Singer, H. J., Rodriguez, J. V., Green, J., Denig, W., Biesecker, D., & Angelopoulos, V. (2015). Space weather conditions during the galaxy 15 spacecraft anomaly. *Space Weather*, *13*(8), 484-502. doi: 10.1002/2015SW001239

Matéo-Vélez, J. ., Paulmier, T., Sicard, A., Dirassen, B., & Payan, D. (2019). Experimental investigation of surface potentials of materials under electron spectra representative of geo and meo worst case environments. *IEEE Transactions on Plasma Science*, *47*(8), 3885-3890. doi: 10.1109/TPS.2019.2925413

Matéo-Vélez, J.-C., Sicard, A., Payan, D., Ganushkina, N., Meredith, N. P., & Sillanpää, I. (2018). Spacecraft surface charging induced by severe environments at geosynchronous orbit. *Sp. Weather*, *16*. doi: 10.1002/2017SW001689

Matéo-Vélez, J.-C., Sicard-Piet, A., Lazaro, D., Inguimbert, V., Sarrailh, P., Hess, S., ... Payan, D. (2016). Severe Geostationary Environments: Numerical Estimation of Spacecraft Surface Charging from Flight Data. *Journal of Spacecraft and Rockets*, *53*(2), 304-316. doi: 10.2514/1.A33376

Mazur, J. E., Fennell, J. F., Roeder, J. L., O'Brien, P. T., Guild, T. B., & Likar, J. J. (2012). The timescale of surface-charging events. *IEEE Transactions on Plasma Science*, *40*(2), 237-245. doi: 10.1109/TPS.2011.2174656

Mazur, J. E., & O'Brien, T. P. (2012). Comment on "analysis of GEO spacecraft anomalies: Space weather relationships" by Ho-Sung Choi et al. *Sp. Weather*, *10*(3), 1–2. doi: 10.1029/2011SW000738

Meier, M. M., Belian, R. D., Cayton, T. E., Christensen, R. A., Garcia, B., Grace, K. M., ... Reeves, G. D. (1996). The energy spectrometer for particles (esp): Instrument description and orbital performance. *AIP Conference Proceedings*, *383*(1), 203-210. doi: 10.1063/1.51533

Mikaelian, T. (2001). Spacecraft charging and hazards to electronics in space. In *Physics of the space environment.*

Mullen, E. G., Gussenhoven, M. S., Hardy, D. A., Aggson, T. A., Ledley, B. G., & Whipple, E. (1986). Scatha survey of high-level spacecraft charging in sunlight. *Journal of Geophysical Research: Space Physics*, *91*(A2), 1474-1490. doi: 10.1029/JA091iA02p01474

O'Brien, T. P. (2009). SEAES-GEO: A spacecraft environmental anomalies expert system for geosynchronous orbit. *Sp. Weather*, *7*(9). doi: 10.1029/2009SW000473

Olsen, R. C. (1983). A threshold effect for spacecraft charging. *J. Geophys. Res.*, *88*(A1), 493–499.

Ozkul, A., Lopatin, A., Shipp, A., Pitchford, D., Mazur, J. E., Roeder, J. L., ... Herschitz, R. (2001). *Initial correlation results of charge sensor data from six intelsat viii class satellites with other space and ground based measurements* (Vol. ESA SP-476). European Space Agency.

Purvis, C., Garrett, H., Whittlesey, A., & Stevens, N. (1984). *Design guidelines for assessing and controlling spacecraft charging effects* (Tech. Rep.).

Rosen, A., Fredricks, R. W., Inouye, G. T., Sanders, N. L., Scarf, F. L., Greenstadt, E. W., ... Sellen, J. M. J. (1972). *Final Report RGA Analysis: Findings Regarding Cor-relation of Satellite Anomalies with Magnetospheric Substorms and Laboratory Test Results* (Tech. Rep.). Redondo Beach, CA, USA.

Rubin, A. G., & Garrett, H. B. (1979). *Ats-5 and ats-6 potentials during eclipse* (Vol. NASA CP-2071). published by NASA, Washington, D.C..

Rubin, A. G., Garrett, H. B., & Wendel, A. H. (1980). *Spacecraft charging on ATS-5* (Tech. Rep.). Hanscom Air Force Base, Mass.: Air Force Geophys. Lab.

Russell, C. T., & McPherron, R. L. (1973). Semiannual variation of geomagnetic activity. *Journal of Geophysical Research (1896-1977)*, *78*(1), 92-108. doi: 10.1029/JA078i001p00092

Saiz, E., Cid, C., & Guerrero, A. (2018). Environmental conditions during the reported charging anomalies of the two geosynchronous satellites: Telstar 401 and galaxy 15. *Space Weather*, *16*(11), 1784-1796. doi: 10.1029/2018SW001974

Sarno-Smith, L. K., Larsen, B. A., Skoug, R. M., Liemohn, M. W., Breneman, A.,

Wygant, J. R., & Thomsen, M. F. (2016). Spacecraft surface charging within geosynchronous orbit observed by the van allen probes. *Space Weather*, *14*(2), 151-164. doi: 10.1002/2015SW001345

Sillanpää, I., Ganushkina, N. Y., Dubyagin, S., & Rodriguez, J. V. (2017). Electron fluxes at geostationary orbit from goes maged data. *Space Weather*, *15*(12), 1602-1614. doi: 10.1002/2017SW001698

Spence, H. E., Blake, J. B., & Fennell, J. F. (1993). Surface charging analysis of high-inclination, high-altitude spacecraft: Identification and physics of the plasma source region. *IEEE Transactions on Nuclear Science*, *40*(6), 1521-1524. doi: 10.1109/23.273510

Stepanov, N., Sergeev, V., Sormakov, D., Andreeva, V., Dubyagin, S., Ganushkina, N., ... Runov, A. (2021). Superthermal proton and electron fluxes in the plasma sheet transition region and their dependence on solar wind parameters. *Journal of Geophysical Research Space Physics*.

Thomsen, M. F., Henderson, M. G., & Jordanova, V. K. (2013, may). Statistical properties of the surface-charging environment at geosynchronous orbit. *Sp. Weather*, *11*(5), 237–244. doi: 10.1002/swe.20049

Vampola, A. L. (1994). Analysis of environmentally induced spacecraft anomalies. *Journal of Spacecraft and Rockets*, *31*(2), 154-159. doi: 10.2514/3.26416

Whipple, E. C. (1981). Potentials of surfaces in space. *Reports on Progress in Physics*, *44*(11), 1197–1250. doi: 10.1088/0034-4885/44/11/002

Wrenn, G. L., & Smith, R. J. K. (1996). Probability factors governing ESD effects in geosynchronous orbit. *IEEE Transactions on Nuclear Science*, *43*, 2783–2789. doi: 10.1109/23.556867